The High-Latitude Ionosphere and its Effects on Radio Propagation

R. D. Hunsucker, J. K. Hargreaves

Book DOI: http://dx.doi.org/10.1017/CBO9780511535758

Online ISBN: 9780511535758

Hardback ISBN: 9780521330831

Paperback ISBN: 9780521041362

Chapter

Chapter 5 - The high-latitude F region and the trough pp. 227-284

Chapter DOI: http://dx.doi.org/10.1017/CBO9780511535758.007

Cambridge University Press

Chapter 5

The high-latitude F region and the trough

5.1 Circulation of the high-latitude F region

5.1.1 Introduction

The high-latitude ionosphere is greatly influenced by the outer magnetosphere and the solar wind, the essential connection being via the geomagnetic field. Through this connection the high-latitude F region is exposed to the interplanetary medium and thence to disturbances originating in the Sun. The circulation of the magnetosphere (Section 2.4.1) establishes a corresponding circulation pattern in the high-latitude F region. Although production by solar EUV is still important, these added features lead to a more complex ionosphere, which exhibits some striking differences both from the middle- and from the low-latitude zones. In describing the F region at high latitude, therefore, we shall be particularly concerned with two underlying factors:

(a) the dynamic nature of the high-latitude ionosphere, the pattern of circulation of the F region being mainly controlled by the solar wind and its variations, and

(b) the influence of energetic particles from the magnetosphere and the solar wind, to which the region is generally more accessible than is the ionosphere at lower latitudes.

The auroral zones, which occur within the high-latitude region, are particularly complex, and the *trough* of depleted ionization on its equatorward side has its own pattern of behavior. The present chapter deals with the behavior of the high-latitude F region, its patterns of circulation, and their consequences. The auroral phenomena are discussed in Chapter 6.

5.1.2 Circulation patterns

In the F region the ion–neutral-species collision frequency is small relative to the gyrofrequency, and therefore the plasma moves with the magnetic-field lines rather than with the neutral wind. The motion may also be considered as the motor effect of the cross-polar electric field mapped down from the magnetosphere. The plasma speed **v**, the electric field **E** and the magnetic flux density **B** are related by $v = E/B$ (Equation (2.12)). Since the polar magnetic field is almost vertical, with a value of about 5×10^{-5} Wb m^{-2}, typical plasma speeds of 200–1000 m s^{-1} correspond to electric fields of 10–50 mV m^{-1}.

The integral of the electric field across the polar cap, which may be determined from satellite measurements, provides an estimate of the total electric potential difference across the magnetosphere between its dusk and dawn sides. Various formulae have been derived to express the polar-cap potential (ϕ) in terms of the solar-wind speed (v_{sw}), the total flux density of the interplanetary magnetic field (IMF) (B) and the "clock angle" of the IMF (θ) as seen from the Earth. If B_z and B_y are the northward and westward components of the IMF, then

$$\theta = \tan^{-1}|B_y/B_z| \qquad \text{if } B_z > 0 \text{ (northward)},$$

or

$$\theta = 180° - \tan^{-1}|B_y/B_z| \qquad \text{if } B_z < 0 \text{ (southward)}.$$

A recent analysis (Boyle et al., 1997) gives

$$\phi = 10^{-4} v_{sw}^2 + 11.7 B \sin^3(\theta/2), \tag{5.1}$$

where v_{sw} is in km s^{-1}, B is in nanoteslas, and ϕ is in kilovolts. If $v_{sw} = 400$ km s^{-1} and $B = 5$ nT, the first term gives 16 kV and the second one between 0 and 58.5 kV, depending on the orientation of the IMF. In terms of the magnetic activity index K_p (Section 2.5.4), which is derived entirely from ground-based data,

$$\phi = 16.5 + 15.5 Kp. \tag{5.2}$$

The basic flow pattern caused by the polar-cap electric field is simple enough. The plasma flows from the noon sector to the midnight sector directly over the pole, and there is a return flow around the low-latitude edge of the polar cap, in the vicinity of the auroral oval, and so back to noon. See Figure 5.1(a).

The speed of flow is typically several hundred m s^{-1}. The flow over the polar cap corresponds to the motion of open field-lines from the cusp to the tail (Section 2.4.1), and the return flow corresponds to the sunward flow of closed field-lines down the flanks of the magnetosphere. However the co-rotation effect, conveniently represented by the co-rotation electric field (Section 2.4.4), must also be included, and then the flow pattern becomes distorted as in Figure 5.1(b). The two

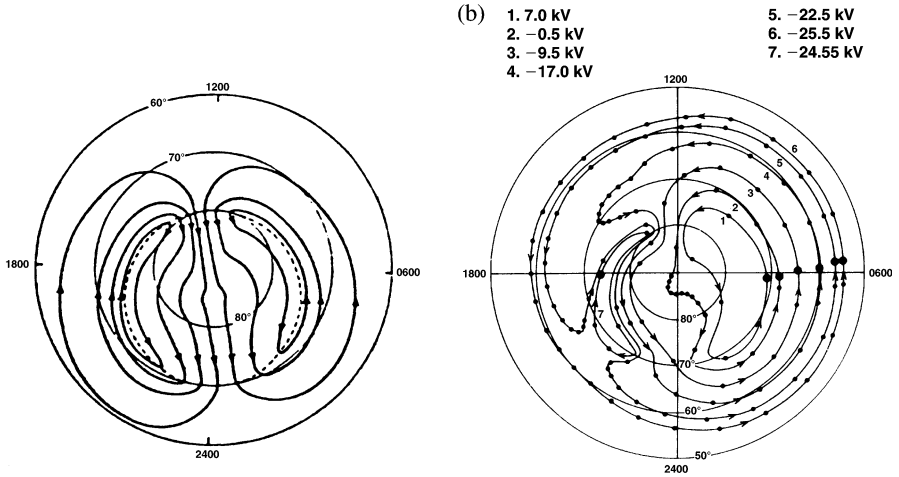

Figure 5.1. Plasma convection at high latitude. (a) Polar convection pattern without co-rotation. (R. W. Spiro *et al.*, *J. Geophys. Res.* **83**, 4255, 1978.) (b) Examples of convection paths of plasma at 300 km altitude in the northern hemisphere under the combined electric fields due to the magnetosphere and co-rotation. The large dots indicate the starting points used in the calculations. The time between successive dots is 1 h, except for the return to the starting point. Each path is an equipotential, whose value is indicated. The boundary of the polar cap is a circle (not marked) of radius 15°, centered 5° towards midnight from the geomagnetic pole. (After S. Quegan *et al.*, *J. Atmos. Terr. Phys.* **44**, 619, Copyright 1982, with permission from Elsevier Science.)

circulation cells are now different, and the evening cell is particularly affected because here the return flow and the co-rotation act in opposite directions. There are some field-lines that follow long, complicated paths, while others may circulate endlessly in small vortices. All these features have ionospheric consequences. In addition the whole pattern is constantly changing in response to variations of the solar wind.

The IMF exerts a major influence on the circulation pattern of the polar ionosphere. Because of the stronger coupling at the magnetopause, the magnetosphere circulates most strongly when the IMF has a southward component (Figure 2.19). This is the situation in Figure 5.1. The control exercised over the drift by the IMF has been proved by measurements of the drift at high latitude at times when satellites were situated in the solar wind just outside the bow shock (Willis *et al.*, 1986; Todd *et al.*, 1986).

There is a more complicated pattern of circulation when the IMF is northward, but its nature has been more controversial. Various two-, three-, and four-cell patterns have been proposed. Several agreed features distinguish it from the pattern for southward IMF.

(1) It is more structured, but the speeds are lower.

(2) The region of moving plasma is restricted to higher latitudes.

(3) There is a region of sunward convection at the highest latitudes.

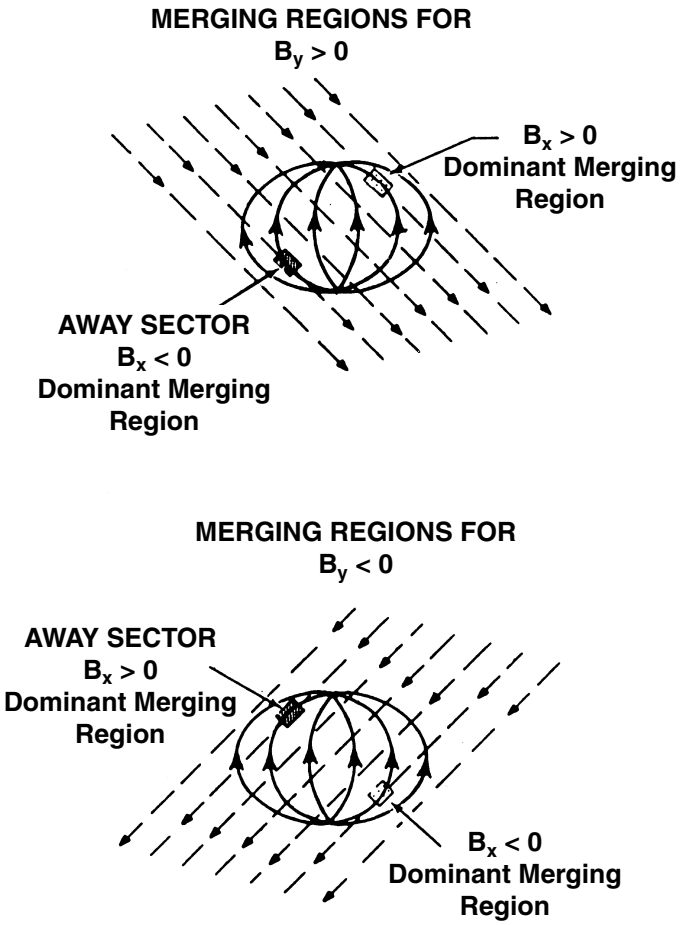

Figure 5.2. Geometry of the IMF and the geomagnetic field viewed from the Sun. Regions of preferred merging for various orientations of the IMF are indicated by shaded boxes. The principal merging region changes its location according to the "Sun–Earth" (B_x) and "east–west" (B_y) components of the IMF. (R. A. Heelis, *J. Geophys. Res.* **89**, 2873, 1984, copyright by the American Geophysical Union.)

The east–west component of the IMF (usually called B_y) also affects the circulation, presumably because of shifting connection regions at the magnetopause (Figure 5.2).

Figure 5.3 shows versions of the circulation patterns of the northern polar region according to the directions of the north–south and the east–west components of the IMF. Versions (a) and (b) agree that the circulation is generally weaker when B_z is positive (i.e. northward), though the details differ. The influence of the east–west component over the form and size of the cells is clear in version (a) but less so in version (b). The latter shows two-cell patterns throughout, whereas in (a) three- or four-cell patterns appear when the IMF is northward.

Rich and Hairston (1994) have made a comprehensive compilation of poten-

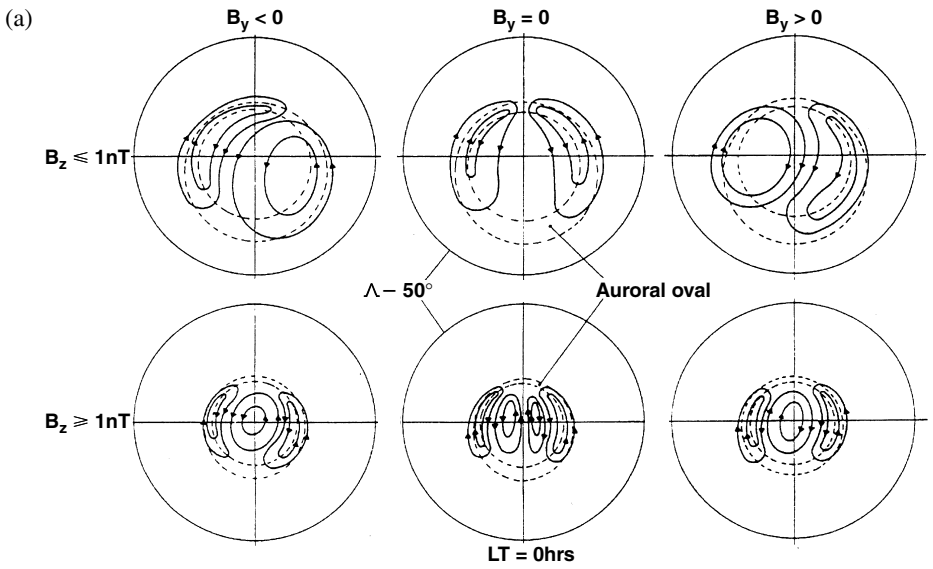

Figure 5.3. Patterns of the circulation of the high-latitude F region in the northern hemisphere for various orientations of the IMF. The viewpoint is that of an observer looking down on the polar region. In each diagram noon is at the top and the geomagnetic pole is in the center. (a) A conceptual picture based on various studies including European incoherent-scatter radar data. (After S. W. H. Cowley and M. Lockwood, *Ann. Geophysicae* **10**, 103, 1992, copyright notice of Springer-Verlag.) The two-cell pattern for southward IMF (top row) gives way to three- or four-cell patterns when it is northward (bottom row). The columns are respectively for when the east–west component is directed towards the west, is zero, and is directed towards the east. (b) Results from a HF radar in North America, for a moderate level of disturbance (K_p from 2− to 3+ inclusive). In these patterns the IMF is northward at the top, southward at the bottom, westward on the left and eastward on the right. (J. M. Ruohoniemi and R. A. Greenwald, *J. Geophys. Res.* **101**, 21 743, 1996, copyright by the American Geophysical Union.) The two-cell pattern dominates throughout, though with differing magnitude.

tial distributions (equivalent to flow diagrams) from satellite measurements recorded between 1988 and 1990, divided according to season, and to magnitude and orientation of the IMF. Using advanced ionosondes at polar-cap stations in northern Canada, Jayachandran and MacDonald (1999) find a marked seasonal variation in the flow pattern. When the IMF is southward, the central region of the flow, that which passes over the pole, is observed to be towards magnetic midnight in winter but towards 2000 local magnetic time in the summer, with a gradual transition between. For northward IMF, those times are about 2 h earlier (i.e. 2200–1800 LT). There is (of course!) a considerable spread about these trends on individual days.

The effect of the east–west IMF component should be in opposite directions in northern and southern hemispheres. Cases studied by Dudeney *et al.* (1991) using HF coherent radar (Section 4.2.2) appear to verify this. Lu *et al.* (1994), using

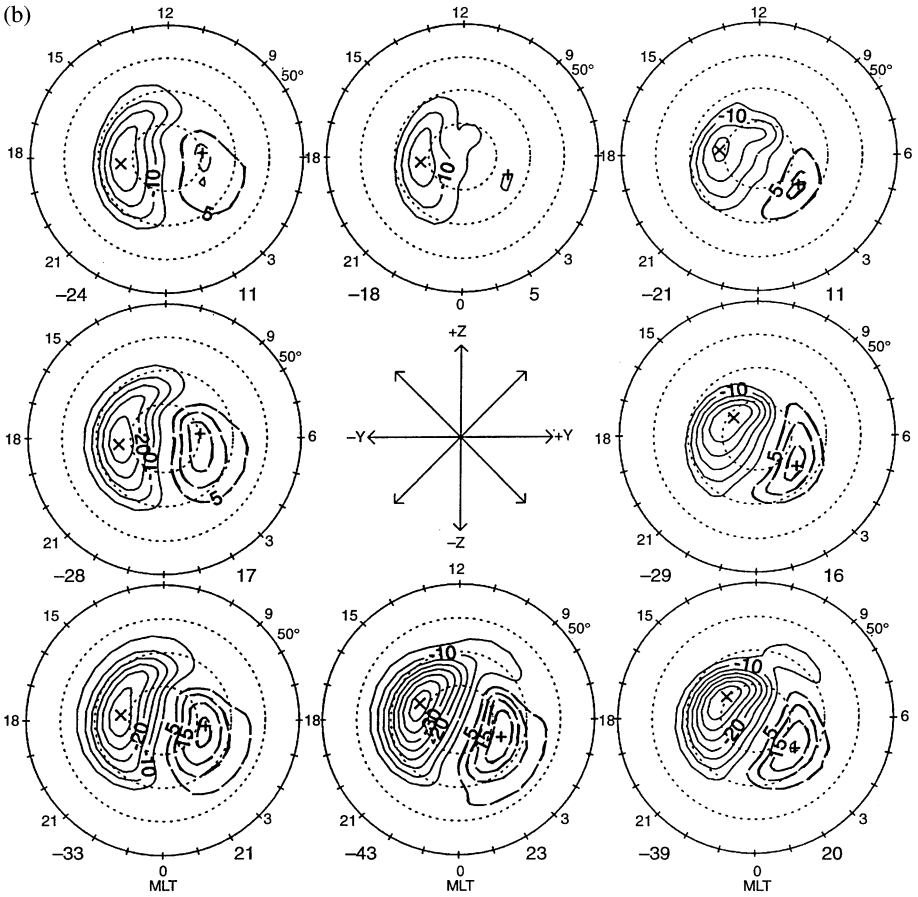

Figure 5.3. (*cont.*)

magnetogram interpretation combined with incoherent-scatter radar, distinguish three cases.

(1) The northern and southern patterns of circulation are mirror images when the IMF is southward.

(2) When the IMF has a northward component that is smaller in magnitude than the east–west component, the patterns are similar to each other but of different intensities.

(3) If the IMF is strongly northward, the patterns in the summer and winter polar caps are very different.

Figure 5.4 illustrates these patterns.

Cowley and Lockwood (1992) point out that the polar circulation is driven by two components, one the dayside coupling between the solar wind and the geomagnetic field, and the other the night-time ionosphere's reaction to changes in

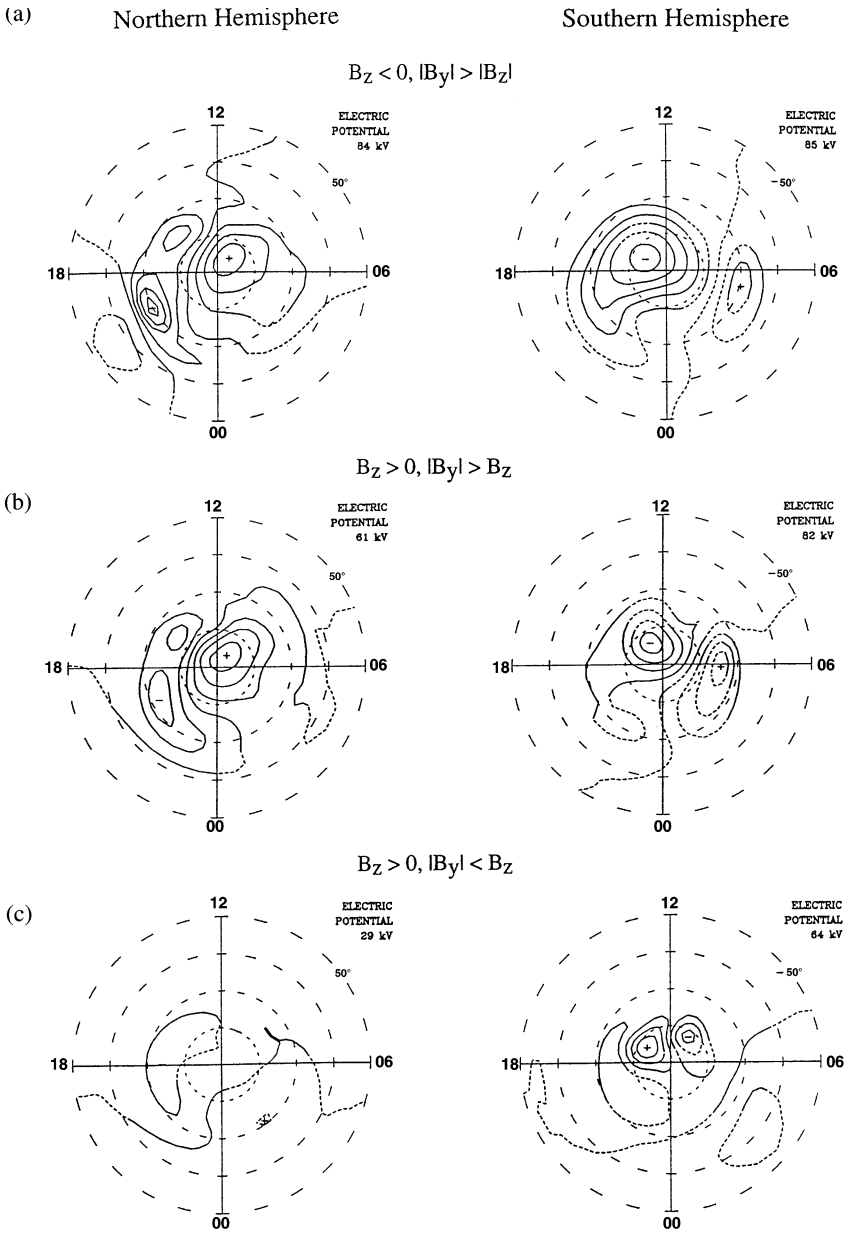

Figure 5.4. Convection in northern and southern hemispheres under various conditions of the IMF: (a) southward component but east–west component larger, (b) northward component but east–west component larger, and (c) northward component with smaller east–west component. The plots show the equipotentials, which are also the streamlines of the polar flow. (G. Lu *et al.*, *J. Geophys. Res.* **99**, 6491, 1994, copyright by the American Geophysical Union.)

the magnetotail. The latter are expected to be delayed 30–60 min behind a change in the IMF. It is not surprising, then, that it takes some time for the circulation to settle into a new pattern following a change in the IMF. According to Hairston and Heelis (1995), analyzing a limited number of cases, a new convection pattern appeared 17–25 min after the IMF turned from northward to southward. For a northward turning the lag was 28–44 min. Since the IMF is always changing to some extent, there will obviously be some times when the polar circulation is in a state of transition and will not conform to any particular model.

A discussion of observations of high-latitude convection is given by Kelley (1989).

There can be an abrupt change of plasma speed, or even a reversal of direction, across the boundaries of circulation cells, particularly when the IMF is northward. The plasma drift is equivalent to an electric field (as measured by a stationary observer), which is communicated along the field-lines to the E region. Therefore the Pedersen current (Section 1.5) in the E region also alters abruptly. To maintain continuity, current then flows up the field lines as a Birkeland current. See Figure 5.5. The corresponding downward flow of electrons is probably the cause of the sun-aligned arcs observed in the polar cap when the IMF is northward (Section 6.3.2).

5.2 The behavior of the F region at high latitude

5.2.1 The F region in the polar cap

The tongue

Figure 5.6 shows F-region critical frequencies measured with ionosondes within the northern polar cap. As would be expected, the values are generally much larger in the sunlit region than they are in the dark. On this occasion there is also a tongue of ionization, drawn out from the day side, over the pole, and into the night sector. This disrupts the pattern that we might have expected, which ought to exhibit a sharp gradient between the sunlit and dark regions. The tongue is most pronounced near the equinoxes, when the terminator crosses the polar cap. The tongue may be broken into dynamic patches, which will be discussed in more detail later in this chapter.

The polar F region is at its most variable when it is at its darkest – during winter, and when the magnetic pole is anti-sunward of the geographic pole. Critical frequencies can be very low: values of f_0F of approximately 2–3 MHz (electron densities from several times 10^4 to 10^5) are common, and $f_0F = 1$ MHz (implying a peak electron density as low as 1.4×10^4 cm^{-3}) has been reported from ionosonde data (Whitteker *et al.*, 1978). The lowest values occur in the dark, anti-sunward, part of the polar cap and generally near local midnight. (Also see Section 5.5.)

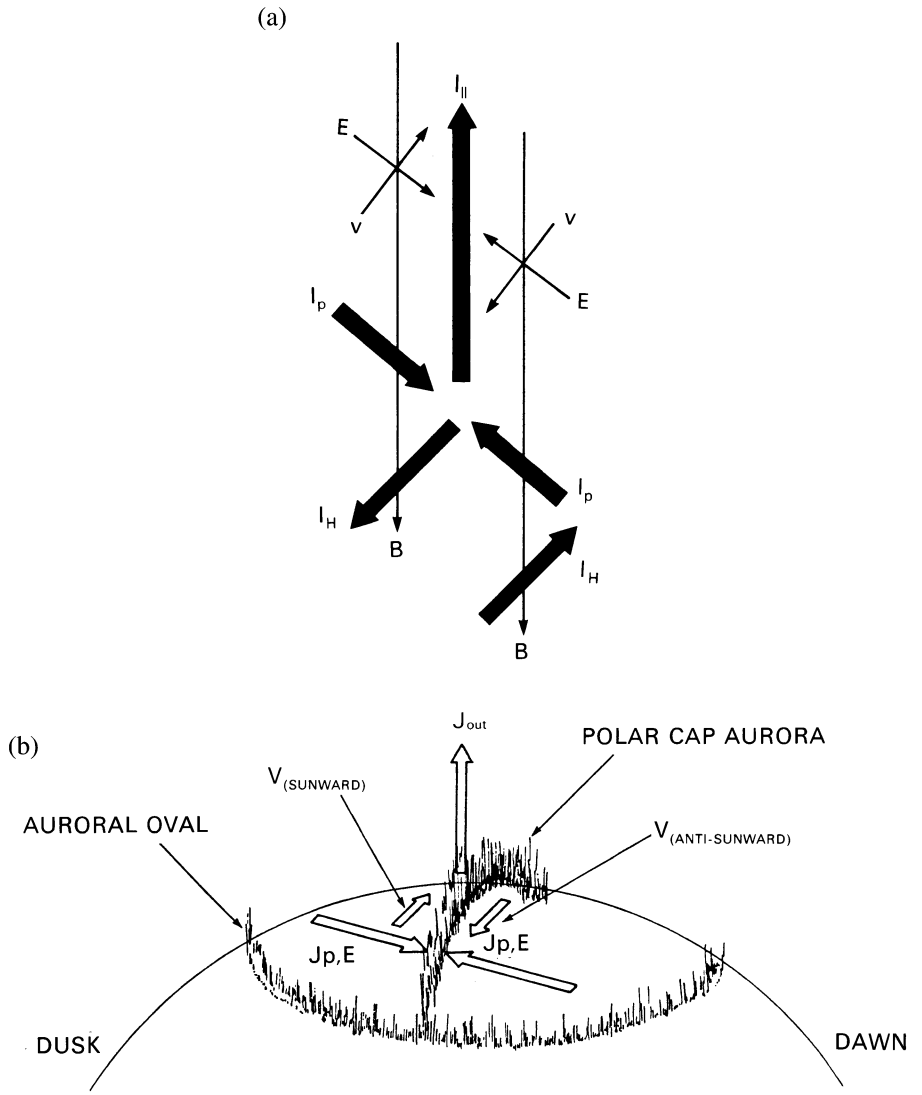

Figure 5.5. (a) Field-aligned current due to velocity shear in a magnetoplasma. **B**, magnetic field; **v**, velocity; **E**, electric field; I_H, I_P, and $I_{||}$: Hall, Pedersen, and field-aligned currents. (b) The field-aligned current associated with the polar-cap aurora at the boundary between circulation cells. (Reprinted from H. C. Carlson *et al.*, *Adv. Space Res.* **8**, 49, copyright 1988, with permission from Elsevier Science.)

The UT effect

A remarkable observation is that the daily variations of the F region depend on universal time as well as on local time. There is, for example, a daily variation at the South Pole, even though the solar zenith angle is virtually constant there over 24 h. The electron density there, as elsewhere in the Antarctic, peaks about 0600 UT, which happens to be near magnetic midnight.

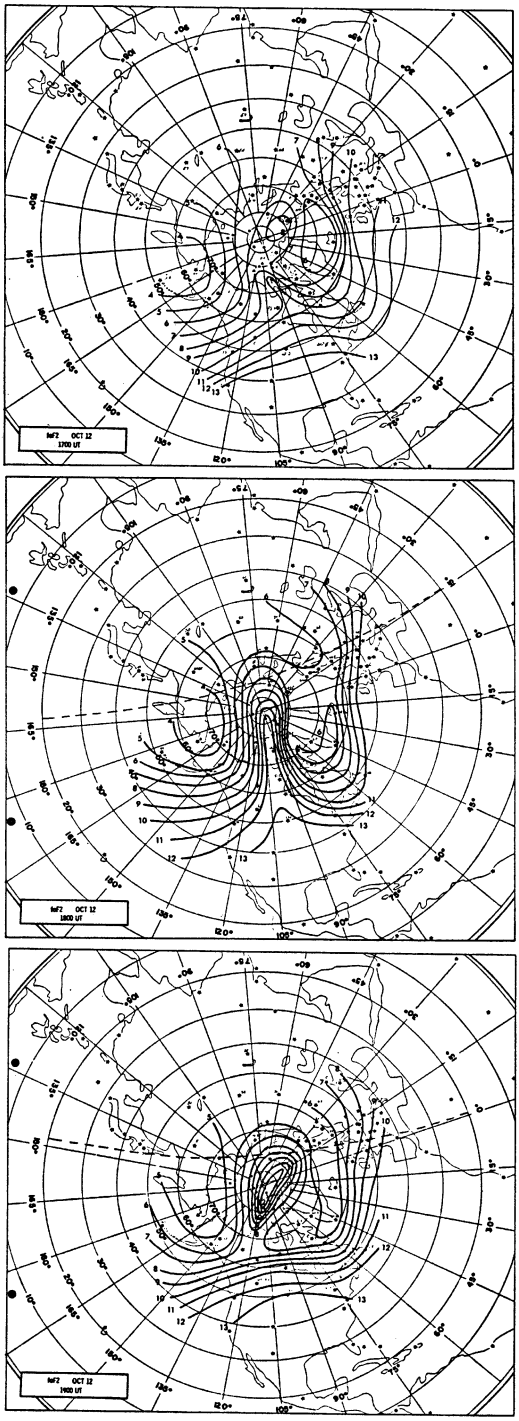

Figure 5.6. Maps of the F-region critical frequency (f_0F2) showing the development of a "sporadic-F" event on 12 October 1957. (G. E. Hill, *J. Atmos. Sci.*, **20**, 492, 1963.) The plots are successively for 1700, 1800 and 1900 UT and the sunlit hemisphere is at the bottom of each plot. The contours range between 4 and 13 MHz.

The explanation of the UT variation depends on the separation of the geographic and magnetic poles. The neutral-air wind in the thermosphere blows over the polar regions generally away from the Sun. At 0600 UT in the Antarctic and 1800 UT in the Arctic the geographic pole is on the midnight side of the magnetic pole, and the drag of the neutral particles against the ions therefore acts to lift the ionosphere (as described in Section 1.3.4). The rate of recombination of ions is thereby reduced and the net ion density is increased. This is also the time of day when the largest amount of the geomagnetic polar cap is sunlit, and it is therefore when the circulation pattern will be most effective at bringing solar-produced ionization over the pole. It is significant that, in the northern hemisphere, where the separation between the poles is smaller, the UT effect is less pronounced than it is in the south.

In the polar cap the F1 layer can be almost as strong as the F2 layer, and on occasions it may be even stronger. This produces the so-called "G condition" on ionograms.

5.2.2 The effect of the polar cusps

On the day side of the Earth are two regions, one in each hemisphere, where the geomagnetic field-lines provide a direct connection between the ionosphere and the magnetosheath (Section 2.2.5). In the simplest models of the magnetosphere, in which there is no circulation, they correspond to the neutral points on the surface of the magnetosphere. Field-lines at lower latitude are closed, whereas those at higher latitude are "open", connecting with the solar wind and the IMF or sweeping back into the magnetotail. In more realistic, dynamic, models (Sections 2.4.1–2) the cusps are where the dayside field-lines open before being swept over the poles (Figure 5.7(a)). The cusps are significant regions of the magnetosphere and also of the ionosphere.

In the ionosphere the cusp regions have several signatures.

(1) Charged particles with energies similar to those in the magnetosheath may be detected. Whereas the cusps are typically located near $\pm 78°$ geomagnetic latitude, and are about 5° wide, the particle observations show the cusps extending over all daylight hours and merging into the auroral oval (Section 6.2.1). There is also a second, smaller, region extending only a few hours from local noon. The particle flux from the magnetosheath is highly variable over short times (or over small distances, since these observations come from orbiting satellites).

(2) Luminous emissions at 630 nm are enhanced, indicating the occurrence of low-energy excitation of the upper atmosphere. Emissions typical of the aurora (Section 6.3.3) are actually reduced – a feature sometimes called the *noon gap*. These photometric observations reveal a considerable variation in the latitude of the cusp, from 84° under very quiet geomagnetic conditions to 61° under very disturbed conditions.

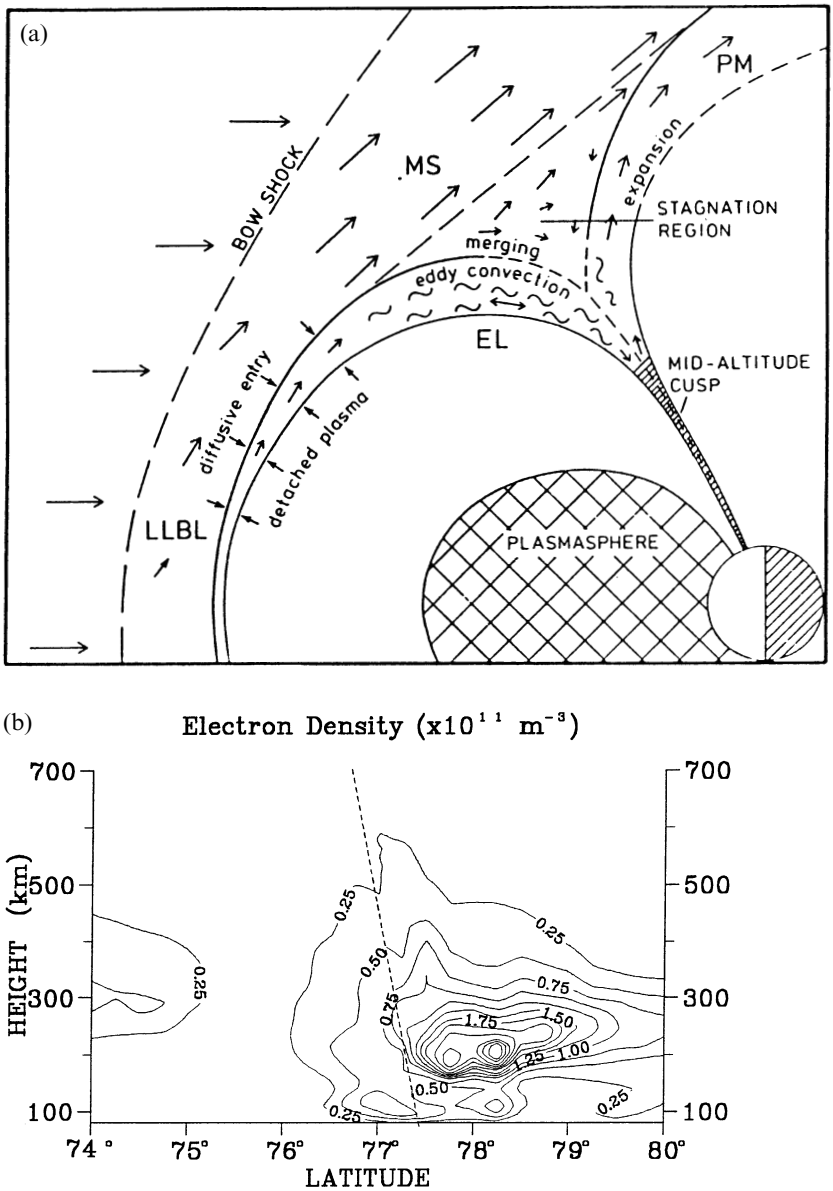

Figure 5.7. Aspects of the polar cusp and its F-region effects. (a) Details of the polar cusp: MS, magnetosheath; LLBL, low-latitude boundary layer; EL, entry layer; and PM, Plasma mantle. (G. Haerendel *et al.*, *J. Geophys. Res.* **83**, 3295, 1978, copyright by the American Geophysical Union.) (b) A tomographic image of the F region on 14 December 1996 at 10:46 UT showing signatures arising from magnetic reconnection. The dashed line marks the boundary between closed and open field-lines, and other features are described in the text. (I. K. Walker *et al.*, *Geophys. Res. Lett.* **25**, 293, 1998, copyright by the American Geophysical Union.)

(3) Owing to the influx of particles from the magnetosheath the density and temperature of the ionosphere is increased and there is a greater degree of irregularity. Owing to the opening of the field-lines, ionospheric plasma may flow out into the magnetosphere, where its ionospheric origin has been recognized from its temperature and composition.

(4) Magnetic pulsations of type Pi2 (of period approximately 30 s) are enhanced. (See Section 2.5.6.)

The image of Figure 5.7(b), which was obtained by the tomography technique (Section 4.4.3), shows features of the F region due to magnetic reconnection at the cusp. The boundary between closed and open field-lines is marked, and, from scanning-photometer observations, Walker *et al.* (1998) were able to identify ionospheric effects due to (1) precipitation of electrons from the ring current on the last closed field-lines, (2) a downward field-aligned current on the first open field-lines, and (3) dispersion of precipitating soft ions on the flux tubes convecting poleward. The last effect shows up as the increasing height of the layer maximum.

5.2.3 The polar wind

The circulation of the magnetosphere carries field-lines from the closed region, through the cusp, and into the polar region where they are open to the solar wind or go deep into the tail of the magnetosphere. These tubes of force lack an effective outer boundary. Furthermore, the scale height is large for light ions at high temperature (Equations (1.3) and (1.46)). Therefore the ionospheric plasma may readily flow upward, and, in the absence of a boundary, the flow may continue as long as the tube remains open.

A steady outward flow is one of the solutions of Equation (1.43), describing the motion of a minority gas under the forces due to a pressure gradient and gravity. As was pointed out in Section 1.3.4, the separation between the heavy ions (oxygen) and the electrons produces an electric field directed upward. When light ions (hydrogen and helium) are also present, they are accelerated by this electric field, which tends to drive them upward. Detailed consideration shows that gravitational attraction is able to bring about a state of hydrostatic equilibrium (Equation (1.47)) in the oxygen ions, but that H^+ is light enough for the electric field to cause the *dynamic equilibrium* state having a steady outflow above some altitude. He^+ may also flow out, though to a lesser extent.

This continuous outflow of light-ion plasma is the *polar wind*. In theory the flow can even reach supersonic speeds, but the details depend on what is assumed about the flow speed at a great distance. The term "polar wind" is sometimes restricted to the supersonic regime, in which case subsonic flow would be a "polar breeze." The flow is limited by collisions with stationary ions, and by the rate of production of H^+ by the charge exchange between oxygen ions and neutral atomic hydrogen (Equation (1.69)) in the topside ionosphere. Since the concentration of

O^+ is far from uniform over the polar cap, the polar wind must be similarly variable.

The lighter ions are the most affected by the outflow, and it is commonly observed in satellite measurements that the concentration of H^+ is greatly reduced relative to the O^+ in the topside ionosphere over the polar caps. The upward speed can be several km s^{-1}. The flux of H^+ is heated by collision with the heavy ions, and its temperature is significantly raised. The theory of the polar wind has been reviewed by Raitt and Shunk (1983). Figure 5.8, from that paper, shows computations illustrating the reduction of topside ion density and the upward drift speed of H^+ for various assumptions about the outer boundary.

One important point established by satellite observations is that the polar wind is a significant source of the plasma in the magnetosphere. That material then convects with the magnetospheric circulation and eventually reaches the plasma sheet at a distance from the Earth that depends on the nature of the ion but is estimated generally to be within $50R_E$. Figure 5.9 illustrates some aspects of the interchange of plasma between ionosphere and magnetosphere.

Plainly, the polar wind is a mechanism that removes ionization from the polar ionosphere from above. Typical loss rates are 3×10^8 cm^{-2} s^{-1} for H^+ ions and 3×10^7 cm^{-2} s^{-1} for He^+. It is secondary to the loss by recombination acting most effectively in the lower F region, and for which electron-content observations lead to estimates in the range 10^9–10^{10} cm^{-2} s^{-1} at middle latitudes.

5.2.4 The F layer in and near the auroral oval

On a long-term view the F region in the auroral zone exhibits properties similar to those typical of middle latitudes. Figure 5.10 shows how the average electron density near the peak of the layer varies diurnally during summer and winter at sunspot maximum and minimum. These measurements are by incoherent-scatter radar at Tromsø, Norway (geographic latitude 69.6° N, invariant latitude 67°, $L=6.5$). The winter anomaly (Section 1.4.5) is seen at sunspot maximum but not at sunspot minimum, which is also the case at mid-latitude. The electron density is larger in the months either side of the winter solstice, indicating the presence of a semi-annual anomaly as well (Farmer *et al.*, 1990).

In addition, there are additional factors that make the ionosphere more irregular in both time and distance. In the poleward part of the auroral oval and extending several degrees into the polar cap, the electron density may be enhanced by the precipitation of low-energy electrons (maintaining the F-region penetration frequency at at least 3 MHz). There may be large variations over short distances, probably due to irregularity in the intensity of the particle precipitation.

The precipitation (of particles with energy $<$300 eV) is particularly strong in the cusp region (75°–80° magnetic), where the penetration frequency may be increased by several megahertz. This precipitation creates irregularities tens of kilometres across, which then break down into smaller structures (tens of metres

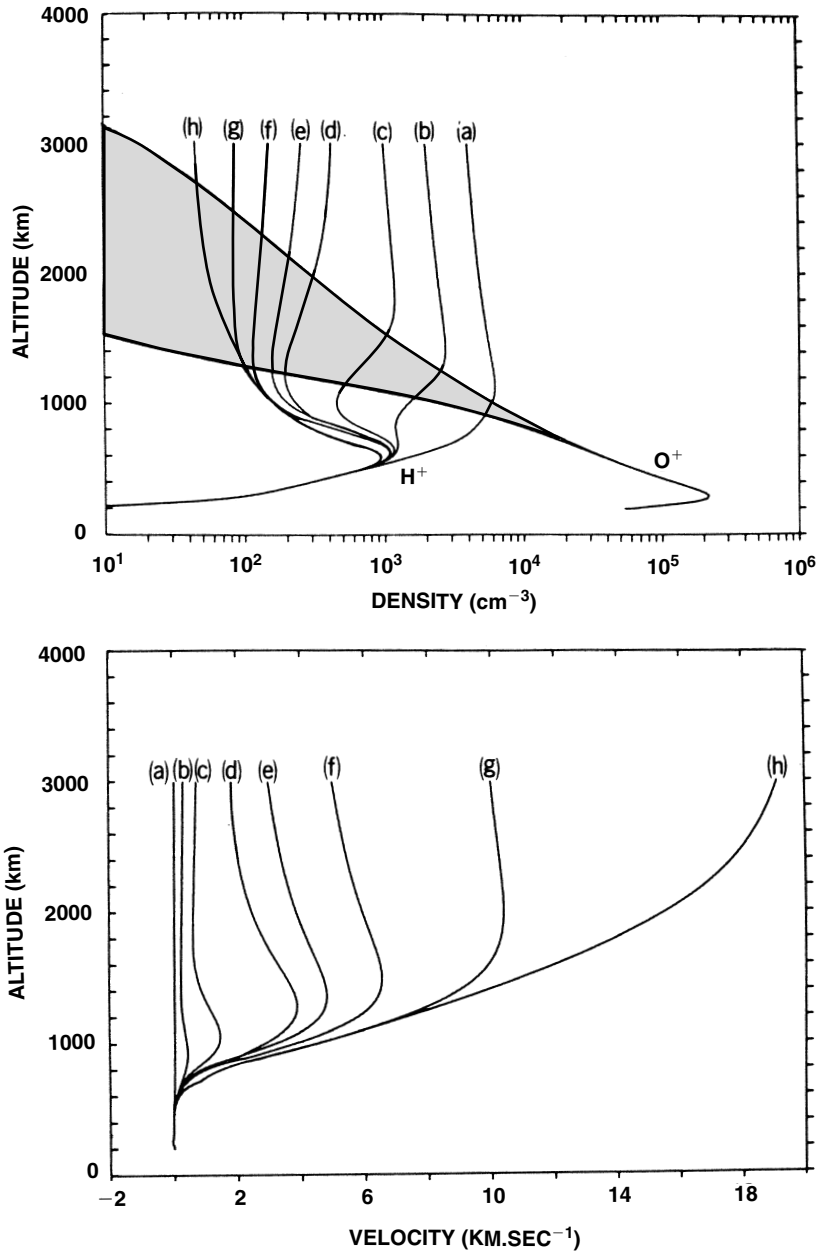

Figure 5.8. Theoretical properties of the polar wind, showing the density of H^+ and the field-aligned drift speed. The various curves are for a range of H^+ escape speeds between 0.06 and 20 km s^{-1} at 3000 km. The range of O^+ is given by the shaded region. (W. J. Raitt and R. W. Schunk, *Energetic Ion Composition in the Earth's Magnetosphere*, Terra Scientific Publishing, Tokyo, 1983, p. 99.)

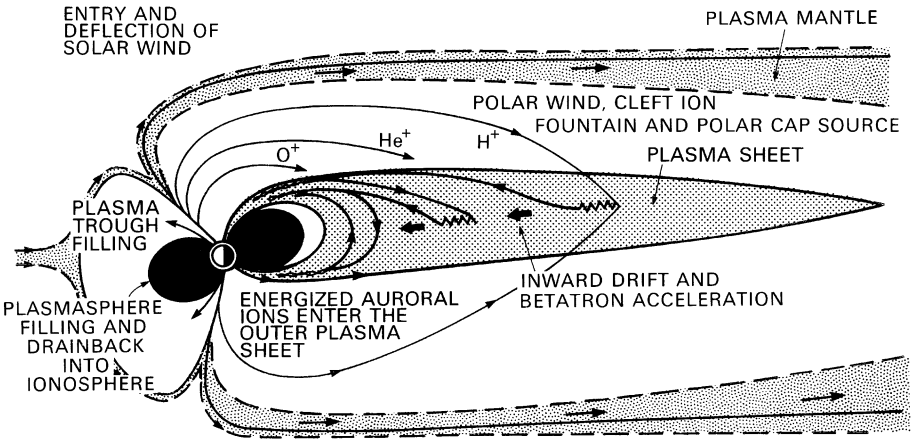

Figure 5.9. Ionospheric sources of plasma for the magnetosphere. Ions leaving the high latitudes tend to separate according to mass. They may subsequently be trapped in the plasma sheet and drift towards the Earth, being energized by betatron acceleration. Computations indicate that the ionosphere is a significant source of magnetospheric plasma. (After C. R. Chappell, *Rev. Geophys*. **26**, 229, 1988, copyright by the American Geophysical Union.)

across or less) as they drift in the general convection (Muldrew and Vickrey, 1982).

No doubt the transport of plasma over the pole also contributes significantly to the ionization observed in the vicinity of the auroral oval near midnight. Structures moving over the pole, provided that they continue to drift in the convection pattern (Figure 5.1), are expected to become distorted on reaching the Harang discontinuity and be diverted eastward or westward along the oval (Robinson *et al.*, 1985). As will be discussed in Section 5.3.2, it is clear from their properties that at least some of the structures in the oval are not of local origin.

On the equatorward side of the auroral oval the F region tends to be depleted of ionization. This is the "main trough", sometimes known by its older name of "mid-latitude trough." The depletion in the trough can be as much as by a factor of ten, though it is often not so great. It is a complex feature, created by the combination of loss processes and the circulation pattern in the region where the high- and mid-latitude ionospheres meet. The trough is considered in detail in Section 5.4.

5.3 Irregularities of the F region at high latitude

5.3.1 Introduction

Spatial irregularities are a common feature of the atmosphere and ionosphere, and their scales of variation cover a wide range in both time and distance. The existence of F-region irregularites has been known for at least 40 years from their

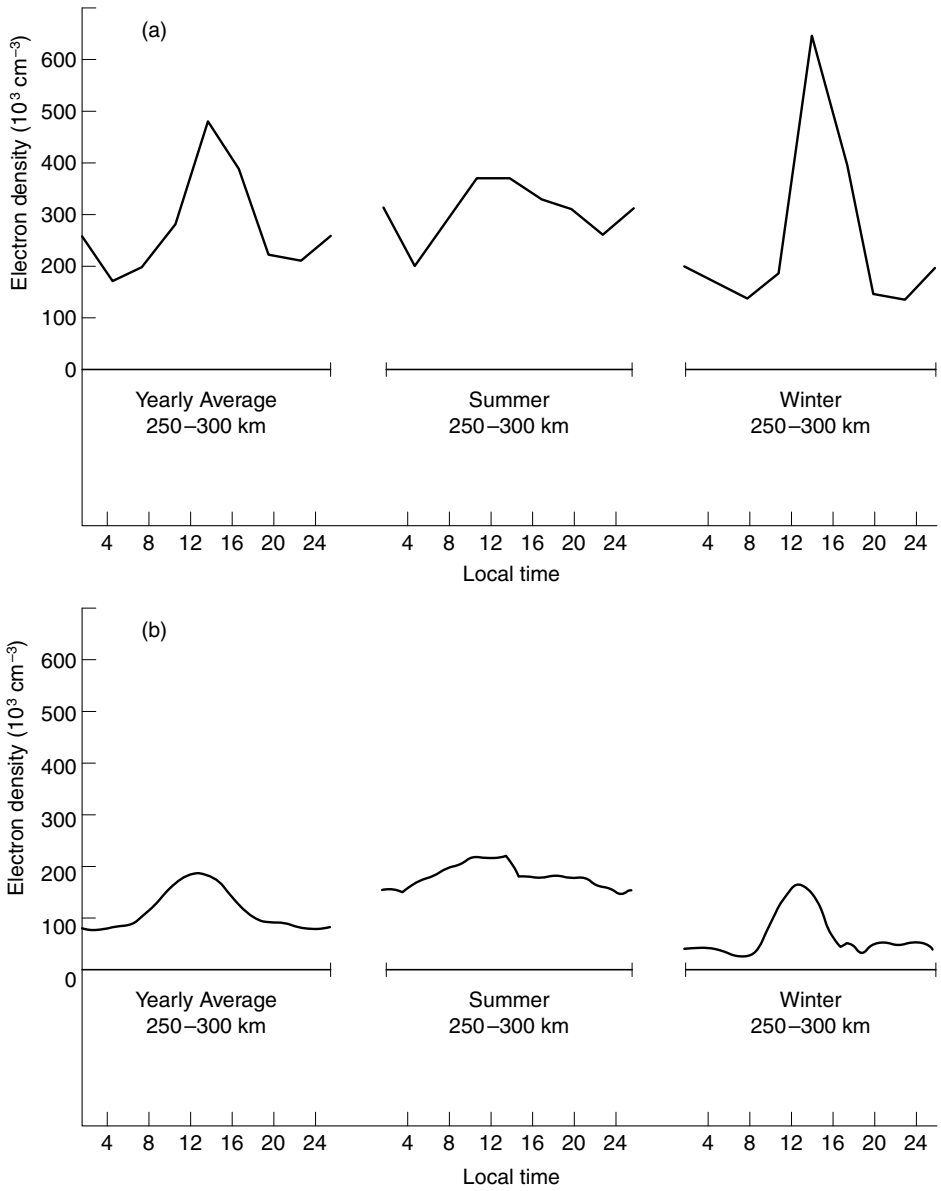

Figure 5.10. Yearly, summer, and winter diurnal variations of electron density near the peak of the F layer at Tromsø. (a) sunspot maximum (August 1981–August 1983), (b) sunspot minimum (April 1986–March 1987). (Reprinted from A. D. Farmer *et al.*, *J. Atmos. Terr. Phys*. **52**, 561, copyright 1990, with permission from Elsevier Science.)

effects on trans-ionospheric radio propagation, originally in observations of radio stars, though our knowledge of them is still incomplete. We are here concerned with the two principal kinds affecting the F region: enhancements extending over tens and even hundreds of kilometers, which can be observed by incoherent-scatter radar and other ionospheric techniques; and irregularities smaller than about 10 km, which, by a diffraction mechanism, produce in propagating radio waves the phenomenon of scintillation.

5.3.2 Enhancements: patches and blobs

We first consider enhancements of large size occurring in the polar cap and the auroral zone. They may be 50–1000 km across and are remarkable for their high plasma density. Even when they are observed during the polar winter night, their density can be more typical of that of the daylit mid-latitude ionosphere. There are several techniques by which they may be observed. Some of the first reports came from polar-cap ionosonde data, when they were described as "sporadic-F." Figure 5.6 showed a good example in which the evolution of a patch may be seen. Speeds of 2000–5000 km h^{-1} (500–1400 m s^{-1}) were reported. The cause of the motion was correctly interpreted as being due to an electric field, but it was (incorrectly) supposed to arise in the E region rather than the magnetosphere.

While much of the information about patches has come from ionosondes, they can also be detected by virtue of the 630-nm airglow which they emit. Other techniques, such as incoherent-scatter radar and tomography, have been significant in the more recent studies of enhancements.

Patches

Enhancements within the polar cap are generally called *patches*. They are seen during the winter night under disturbed conditions, and the F-region electron density may be increased by as much as a factor of ten above the background, which would typically be about 10^5 cm^{-3}. They tend to be stronger at times of high sunspot number.

It seems clear that this type of enhancement is not produced locally, but was formed some distance away and has then drifted in the polar convection to the point of observation. Because the F region decays only slowly by recombination, the lifetime of the patches should be quite long enough for them to cross the polar cap at a speed of several times 100 m s^{-1} (up to 1 km s^{-1}) from a source on the day side. This possibility has been verified by computations that have also demonstrated how a change of polar circulation, for instance due to an increase in the flow of the solar wind or a sudden change in the IMF (Anderson *et al.*, 1988; Sojka *et al.*, 1993), can detach plasma from the dayside cusp region and carry it over the pole into the midnight sector along a path such those shown in Figure 5.1(b). Lockwood and Carlson (1992) have attributed patch creation to the enhanced plasma flow during a flux-transfer event (Section 2.4.2). What happens when the

enhancement reaches the night sector is less clear, but it probably becomes stretched along the auroral zone in the return flow or merges into the mid-latitude ionosphere (Robinson *et al.*, 1985).

Computer modeling of the high-latitude F region (Sojka *et al.*, 1994) suggests that, at the winter solstice, patch formation should be absent between 0800 and 1200 UT and at a maximum from 2000 to 2400 UT. From then until the equinox there should be strong patches all day. In the summer they should be considerably weaker.

While much is still not understood about these larger structures of the polar ionosphere, a number of observational facts have been established about them.

(a) They are roughly circular, and between 200 km and 1000 km in size.
(b) The patches are smaller than the gaps between them, suggesting that we should consider them as enhancements of ionization above a low background rather than as depletions within a higher background.
(c) The degree of enhancement in a typical patch is 2–10 times the ion density of the background.
(d) The gradients at the edges of patches are fairly sharp, on a scale of a few km to about 100 kilometers, and these gradients are the same in all horizontal directions.
(e) The patches appear when the IMF is southward.
(f) They move with the general plasma drift in the polar cap and at the same speed, neither overtaking the general flow nor lagging behind.
(g) They occur during all seasons of the year but more frequently during the winter.

A different pattern is seen in the weaker circulation which occurs when the IMF has a northward component and conditions are less disturbed. At such times the airglow emissions form thin strips with noon–midnight alignment, and these drift slowly across the polar cap in a dusk-to-dawn direction. In these elongated structures the electron density is enhanced by a factor of 5–8 at times of high sunspot number, but by a smaller amount (a factor of two) near solar minimum (Buchau *et al.*, 1983). Figure 5.11 compares the structures typically associated with northward and southward IMF.

Blobs

In the auroral zone the enhancements are generally known as *blobs*. They are smaller than the patches in the horizontal, extending for tens of kilometers rather than hundreds. Some of them peak low in the ionosphere, in the E region or the lower F region. Figure 5.12 illustrates the structures of the ionosphere as seen by two different techniques: (a) was derived by the tomography technique (Section 4.4.3) from electron-content data in the Scandinavian sector, and (b) was obtained by a scanning incoherent-scatter radar (Section 4.2.3) in Alaska. The upper panel

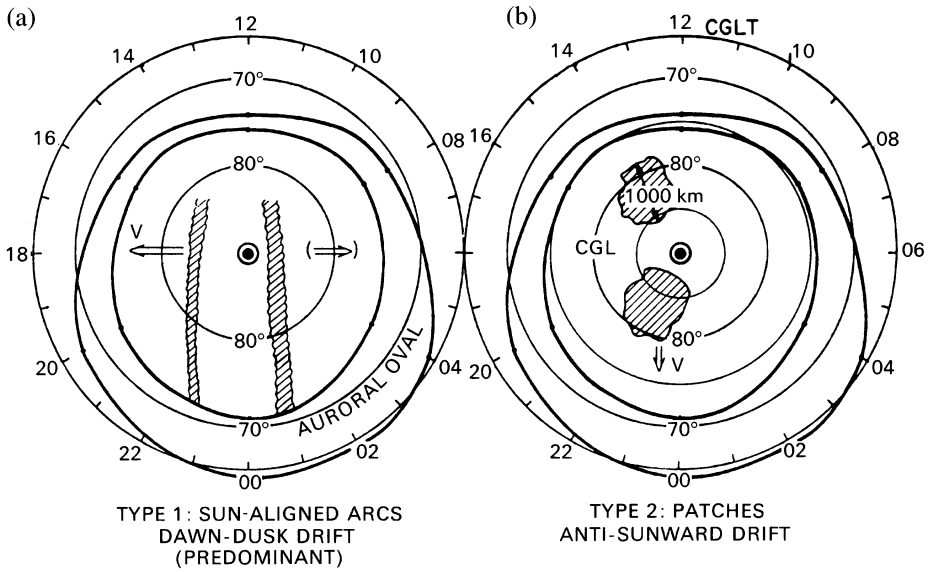

Figure 5.11. Typical irregular structures of the polar F region. (a) arcs with noon–midnight alignment and dusk–dawn drift during northward IMF ($B_z > 0$), and (b) patches drifting towards midnight during southward IMF ($B_z < 0$). The coordinates are corrected geomagnetic latitude (CGL) and local time (CGLT), and the heavy lines mark the auroral oval (Section 6.2). (After H. C. Carlson, private communication.)

gives an overall view showing the mid-latitude ionosphere on the left, the more structured auroral region on the right, and the main trough (Section 5.4) in between, while the two lower panels show similar features as contour diagrams emphasizing the irregularities.

There is some uncertainty about the cause of blobs in the auroral zone. They seem to vary greatly in size. There is some evidence, though it is perhaps not yet definitive, that they move with the plasma drift of the auroral F region as a whole. It seems clear that more than one source is involved, since, as Figure 5.13 illustrates, they may occur over different altitude ranges. Moreover, those at the higher levels are generally cooler than their surroundings by about 10%, whereas those peaking in the lower F region tend to be hotter by about 20%. (According to the results of Burns and Hargreaves (1996), typical electron temperatures are about 1280 and 1540 K, repectively, for the two types, compared with about 1410 K for the plasma outside the blob – all these values being medians over a number of separate determinations.) It is generally assumed that the higher structures arrive as patches drifting from the polar cap (since they are also cooler than their surroundings), but the exact connection and the mechanism which breaks them up are unknown. Those blobs which are hotter and appear at lower altitudes are more likely to have been produced by particle precipitation nearer to the point of observation. Figure 5.12 shows one of these lower blobs, and also examples of the *boundary blob* which is situated just poleward of the main trough. The boundary blob is a long-lived feature that may continue for several hours.

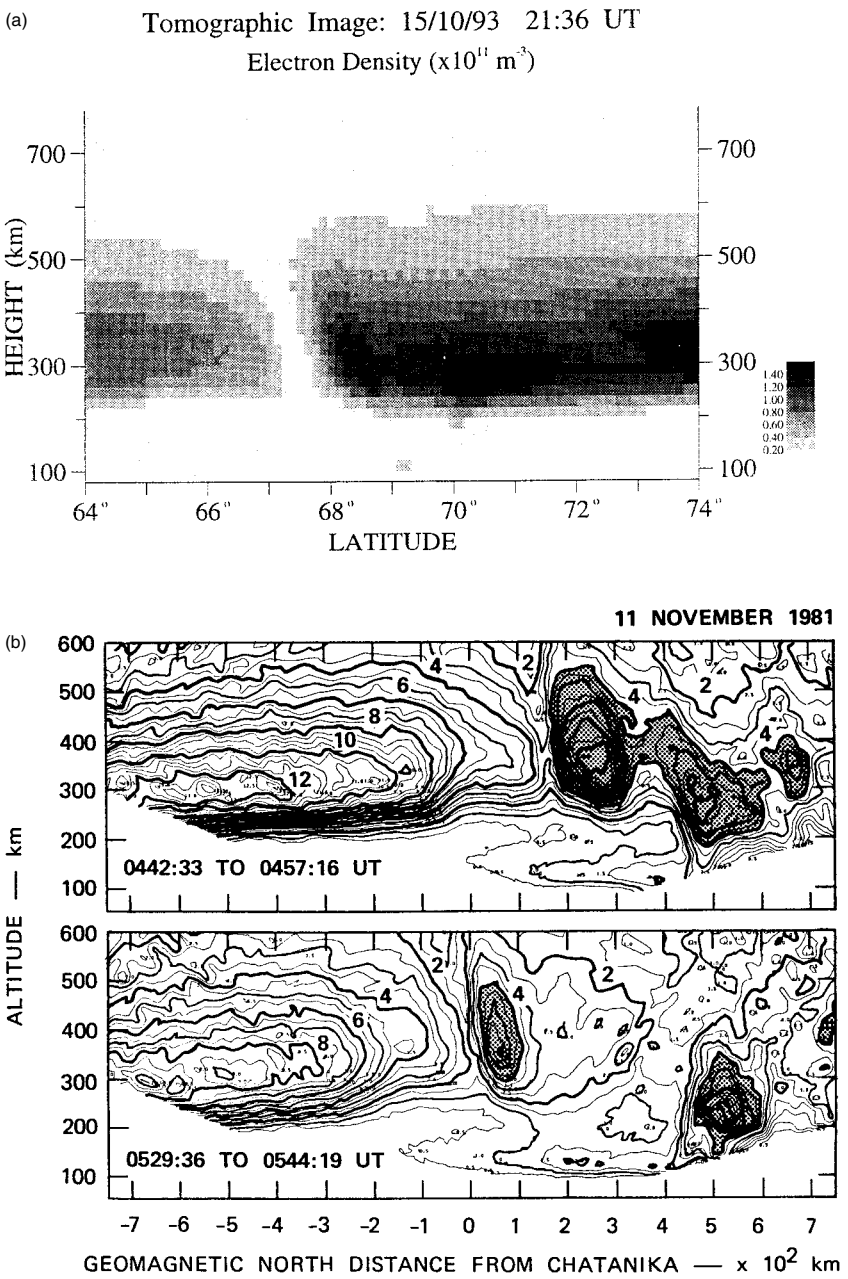

Figure 5.12. (a) A tomographic image of the ionosphere in the Scandinavian sector, 15 October 1993, pre-midnight, showing the mid-latitude ionosphere, the main trough (Section 5.4), and the structured auroral ionosphere. (L. Kersley, private communication, 1998.) (b) Blobs and other features observed with the Chatanika incoherent-scatter radar on 11 November 1981. The time of each scan is marked, and the main trough, a boundary blob, an auroral blob, and the auroral E layer (Section 6.5.4) may be seen from south to north. A distance of 100 km is about 0.9° of latitude. Since Alaskan time is UT – 10 h, these are in the early evening. (C. L. Rino *et al.*, *Radio Sci.* **18**, 1167, 1983, copyright by the American Geophysical Union.)

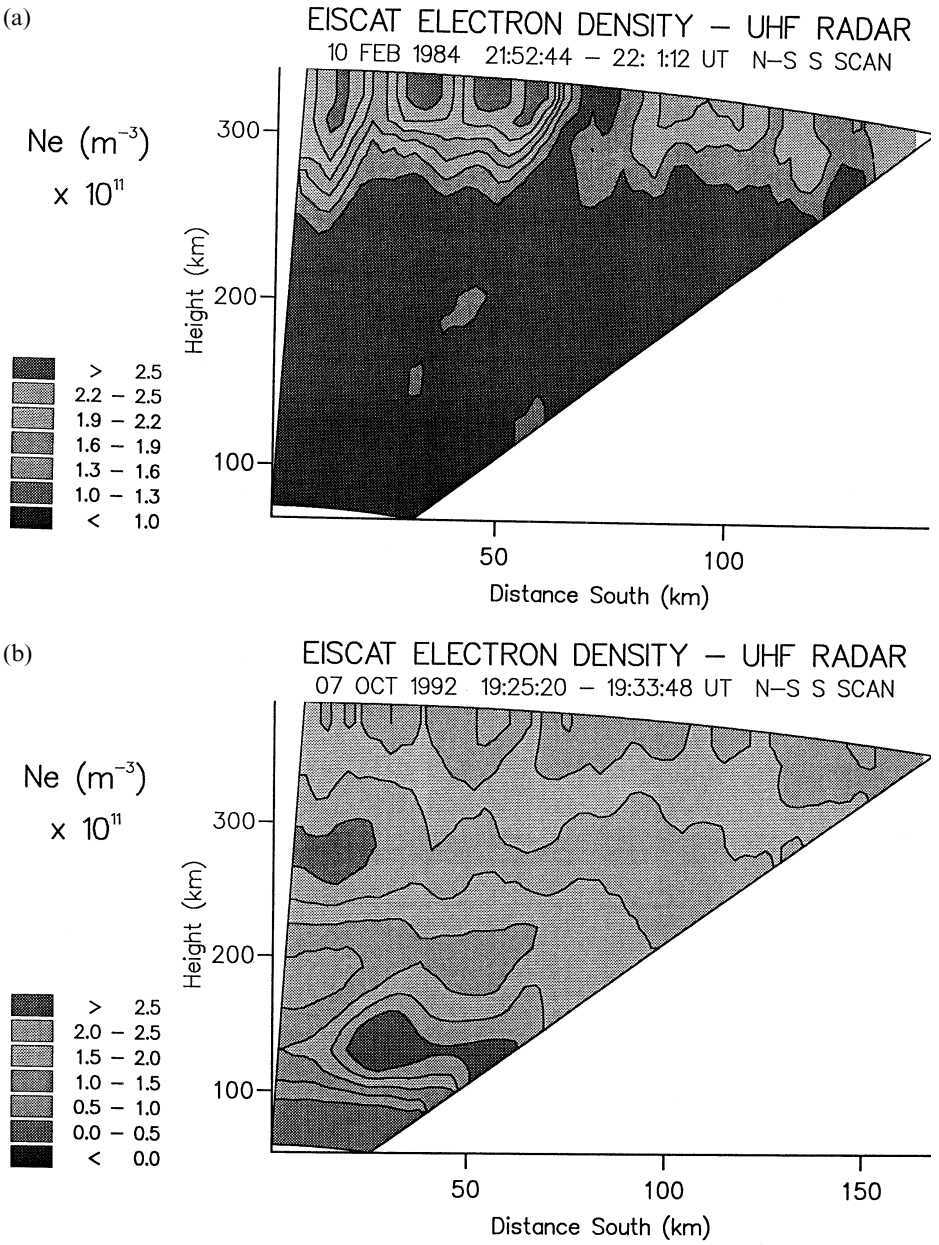

Figure 5.13. Three kinds of blob observed with the EISCAT incoherent-scatter radar. (a) F-region enhancement peaking at 250–400 km (cooler than the surroundings). (b) an intermediate type having an F-region peak and related E-region structure, and (c) a low-altitude blob peaking below 200 km (hotter than the surroundings). (Reprinted from C. J. Burns and J. K. Hargreaves, *J. Atmos. Terr. Phys.* **58**, 217, copyright 1996, with permission from Elsevier Science.)

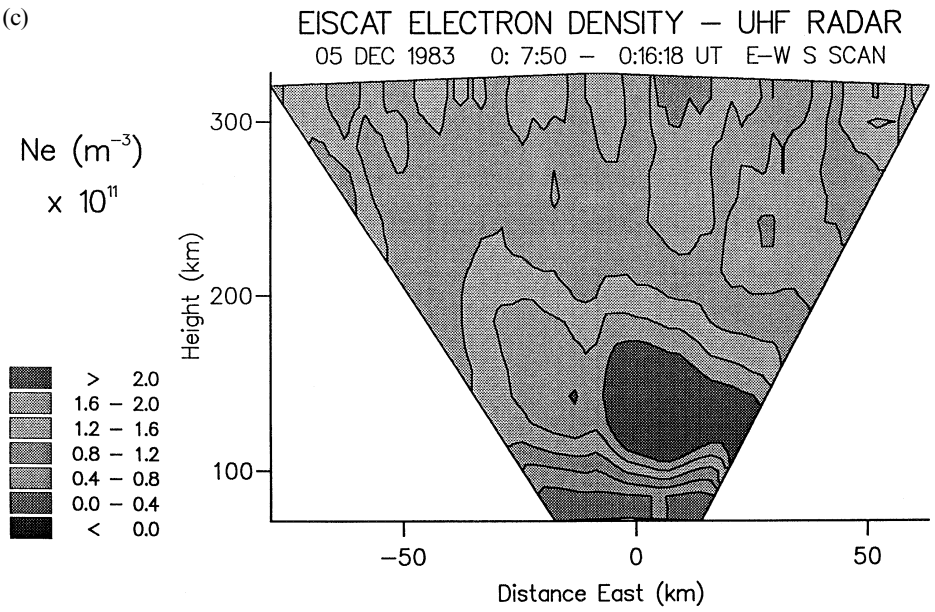

Figure 5.13. (*cont.*)

Table 5.1 compares the main properties of the various types of enhancement.

A comprehensive review of high-latitude enhancements of the F region was made by Tsunoda (1988). A collection of relevant papers was published as a special section of *Radio Science* (1994).

5.3.3 Scintillation-producing irregularities

The irregularities of smaller scale produce scintillation phenomena in trans-ionospheric radio signals. The theory of scintillation was outlined in Section 3.4.5, where it was seen that the radius of the first Fresnel zone is an important parameter. For a radio frequency of 100 MHz the first Fresnel zone has a radius of about 1 km if the effective diffraction screen is at a height of 300 km; therefore irregularites smaller than about 1 km produce both amplitude and phase scintillation. Irregularities larger than that produce phase scintillation only.

Distribution and occurrence

Scintillation occurs at all latitudes, including the polar region, but it tends to be particularly severe at and around the auroral zone (Aarons, 1982; Yeh and Liu, 1982). See Figure 5.14. (The other region of heavy scintillation is at the equator.) The auroral scintillation zone is offset from the magnetic pole and exhibits a general correspondence to the auroral oval (Sections 6.2.1 and 6.3.5), being nearer to the equator in the night sector. Both in the auroral and in the polar regions the

Table 5.1. *A summary of large-scale, irregular structures at high latitude*

Type of irregularity	Location	Typical size	Magnitude	Altitude	Duration	Origin	Motion
Polar cap patches Buchau *et al.* (1983; 1985) Weber *et al.* (1984; 1986) Weber and Buchau (1985)	Polar cap when B_z is south and $K_P > 4$.	100s to 1000s of km horizontal extent. 500 km radius.	$>10^6$ cm^{-3}, about eight times the background F layer	F region	2–3 h	Sub-auroral latitudes equatorward of the dayside cusp. Plasma produced by solar EUV.	Anti-sunward through the polar cap at 250–700 m s^{-1}
Boundary blobs Kelley *et al.* (1980) Vickrey *et al.* (1980) Muldrew and Vickrey (1982) Rino *et al.* (1983) de la Beaujardiere and Heelis (1984) Robinson *et al.* (1985)	Equatorward boundary of the auroral zone. In the midnight sector and extending to the morning and evening.	Extreme longitudinal extent but confined to 100 km in latitudinal width.	$>4\times 10^5$ cm^{-3}	300 to 500 km	Very persistent, >12 h	Either reconfigured patches or semi-permanent structures enhanced by soft particle precipitation	Move equatorward with time, and sunward along the equatorward boundary of the auroral zone
Auroral blobs Rino *et al.* (1983) Robinson *et al.* (1984) Hargreaves *et al.* (1985a; 1985b)	Auroral zone in the night sector and post-noon sector.	Field-aligned 10–100 km north–south, a few times 100 km east–west. Wavelike structure of wavelength about 15 km.	3×10^5 cm^{-3}	Between <200 and >350 km. Isolated blobs near 700 km.	Intermittent, about 1 h	Poleward auroral boundary. Soft particle precipitation and possibly 'spatial' resonance. Source of wavelike structures is unknown.	Zonal drift 250 m s^{-1}
Sun-aligned arcs Weber and Buchau (1981) Carlson *et al.* (1984)	Polar cap. Aligned with the noon–midnight meridian. B_z north.		2×10^5 cm^{-3}			'Polar shower' precipitation in the central polar cap.	Slow dawn-to-dusk movement

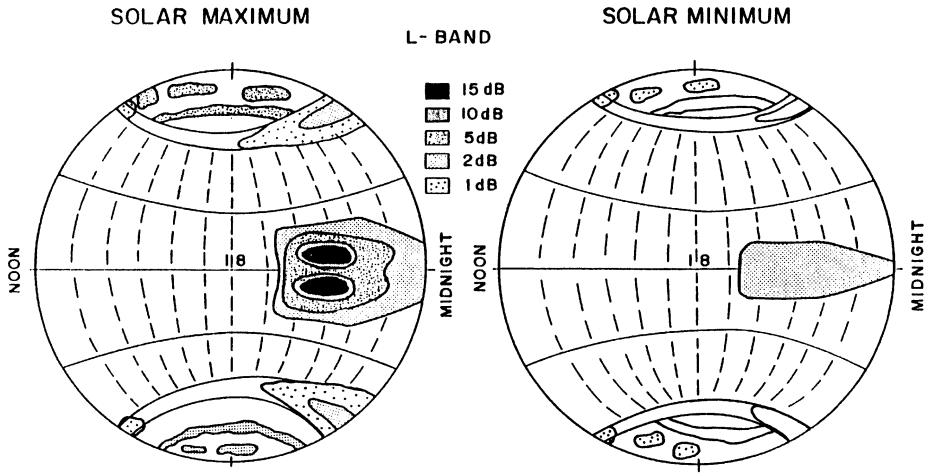

Figure 5.14. The principal regions of scintillation at L band (1.6 GHz). (S. Basu *et al.*, *Radio Sci.* **23**, 363, 1988, copyright by the American Geophysical Union.)

rate of occurrence and the intensity maximize at night, and there is also a daytime maximum in the auroral region only. The seasonal variation depends on the longitude. Figure 5.15 shows the seasonal and daily occurrence patterns for an auroral station in the European sector (Kiruna). The occurrence and the intensity of scintillation increase strongly with the sunspot number; the occurrence also increases with magnetic activity (K_p), but this effect is only slight in the polar cap.

The period and depth of fading

The period of fading varies considerably, but is generally in the range of seconds to a few minutes. It depends on the apparent motion of the irregularities as well as on the depth of the fading. Figure 5.16 shows an example of amplitude scintillation.

The intensity of amplitude fading is commonly measured using the index S_4 (defined in Section 3.4.5). In these terms it depends on the radio frequency as $f^{-1.5}$ if the fading is not too severe, but less steeply for strong scintillation.

The observed depth of scintillation also depends on the direction of propagation between the sender and the receiver (for instance from a satellite to a ground station). Increasing obliquity tends to make the fading more severe because the ray traverses a longer path through the ionosphere, thereby encountering more irregularity in total. Details depend on the form of the individual structures. It may be assumed that there will be considerable elongation along the geomagnetic field, and, according to Rino (1978), auroral irregularities are extended east–west, giving a sheet-like form. Since individual irregularities are strongly field-aligned, there is another maximum for rays traveling directly along the direction of the magnetic field (because rays traveling almost directly along the magnetic field tend to remain within a single irregularity). These effects may be seen in Figure 5.15.

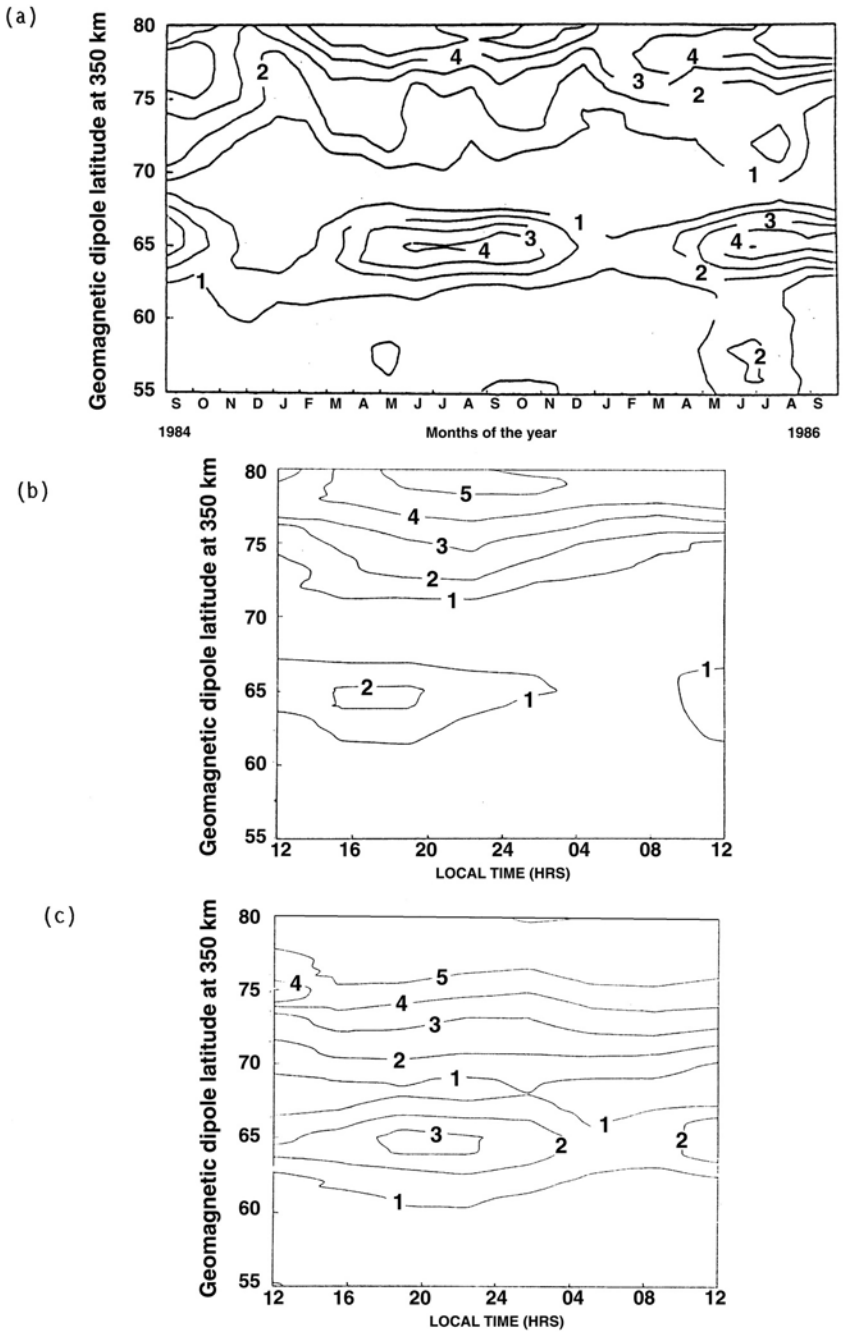

Figure 5.15. The occurrence of scintillation over magnetic latitudes 55°–80° observed from Kiruna (64.3° N, 102.8° E CGM), September 1984–September 1986. The contours show the percentage of time for which the scintillation at 150 MHz exceeded $S_4 = 0.2$. The contours 1–5 represent 25%, 35%, 45%, 55% and 65% respectively. (a) Variation with month. Note the summer maxima. (b) Variation with local time, low magnetic activity ($K_p \leqslant 1$). (c) Variation with local time, moderately high magnetic activity ($K_p \geqslant 4$). (L. Kersley *et al.*, *Radio Sci.* **23**, 320, 1988, copyright by the American Geophysical Union.)

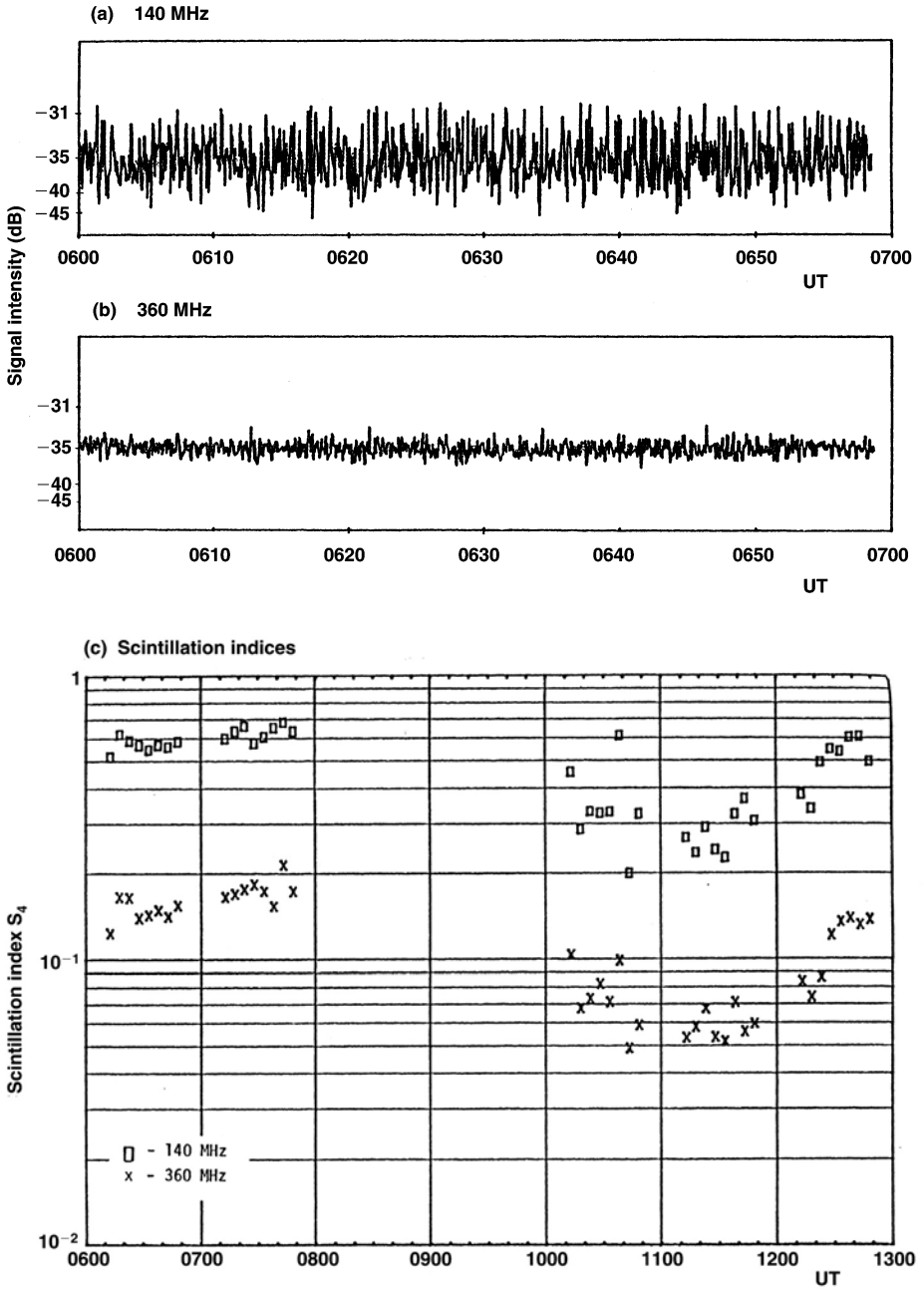

Figure 5.16. Examples of scintillation fading observed in Alaska in transmissions at (a) 140 MHz and (b) 360 MHz from a geosynchronous satellite (ATS-6), on 30 March 1979. The satellite was at low elevation to the south, and the raypath crossed the F region at about 60° geomagnetic latitude. The fading is considerably greater at the lower frequency, with a ratio of almost four between the scintillation indices (c).

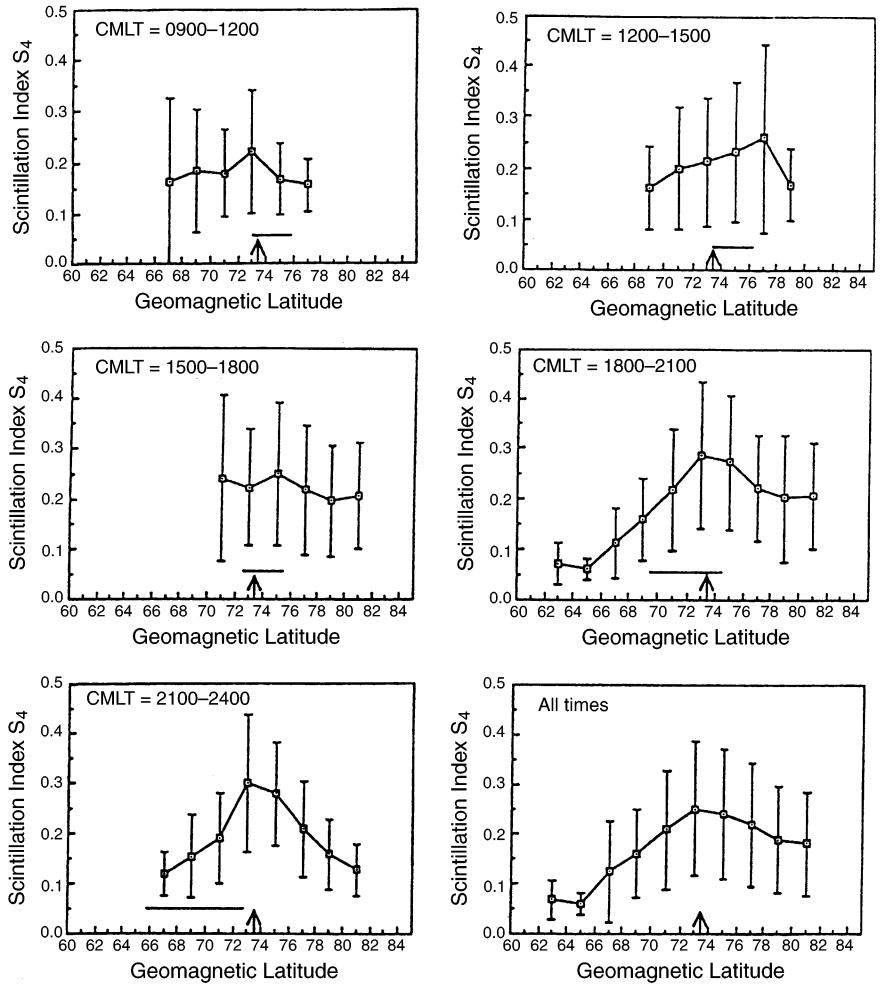

Figure 5.17. The S_4 scintillation index at Hornsund, Svalbard (invariant latitude 73.4° N) at various local magnetic times. The bars indicate the standard deviation. The latitude of the receiving station is marked with an arrow, and horizontal lines indicate the typical latitude of the auroral oval at that time of day. (A. W. Wernick *et al.*, *Radio Sci.* **25**, 883, 1990, copyright by the American Geophysical Union.)

Average values of S_4 at 137 MHz over a range of latitude and at various times of day (geomagnetic local time) are shown in Figure 5.17. All these measurements were made between autumn and early summer (October to May) at Hornsund, Svalbard (invariant latitude 73.4°), whose position is marked on the plots with an arrow. Since the magnetic field is nearly vertical over the polar cap, the propagation path is closest to the magnetic-field direction when the satellite is at the same latitude as the receiving station. The maximum in S_4 at the latitude of Hornsund is clearly present at night.

A value of S_4 equal to 0.25 corresponds to fading with about 1 dB standard

deviation. However, the fading may be much more severe on occasion, and especially so in the auroral zone. Table 5.2 shows the incidence of intense scintillation at the auroral station Narssarssuaq (Greenland) at two radio frequencies.

Note that severe fading is considerably more common under magnetically disturbed conditions and at night. At the highest latitudes (>82° magnetic latitude) the scintillation is associated with polar arcs (Section 6.3.2), and fading of more than 28 db (peak–peak) has been observed at 250 MHz.

Spectrum

The irregularities causing scintillation may be considered as an irregular, spatial distribution that is drifting but also evolving in time. The temporal variation observed at a single site includes the intrinsic time variation, but the main part of the variation is likely to be due to the relative motion between the irregularities and the probing signal. A satellite in low orbit converts the spatial spectrum along the orbit to a temporal spectrum according to the orbital speed. In the case of a geostationary satellite, the temporal change arises from the drift of the irregularities through the satellite-to-ground ray.

Examples of the intensity spectrum of 137-MHz scintillations recorded at Hornsund are shown in Figure 5.18. Since the transmitting satellite, HiLat, was in orbit at an altitude of 800 km, we expect that the time variation will be due mainly to the motion of the satellite across the spatial irregularities – though exact conversion would require knowledge of the irregularity motion as well. The large maxima in Figure 5.18 are due to the effect of diffraction (Section 3.4.5), which prevents large-scale phase irregularities generating amplitude scintillation at the ground. The peak marks the Fresnel frequency. The falling part of the spectrum represents a range of spatial size from about 700 to 130 m (when the satellite is overhead). These are power-law spectra, as is commonly the case, and, in the Hornsund data set, the average spectral index, q, is generally between 2 and 3. That is, for a factor of ten in fading frequency the intensity declined by a factor between 100 and 1000 (20–30 dB). Amplitude fading tends to be dominated by the Fresnel frequency.

Table 5.2. *Depth of scintillation at Narssarssuaq*

	Percentage occurrence			
	⩾12 dB at 137 MHz		⩾10 dB at 254 HMz	
K_p	Day	Night	Day	Night
0–3+	2.9	18	0.1	2.6
>3+	19	45	0.9	8.4

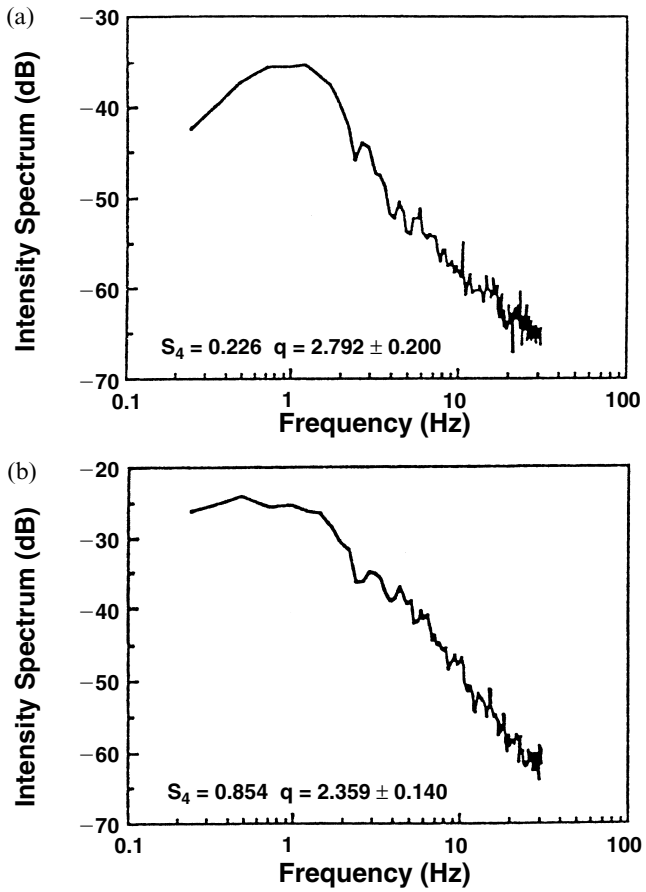

Figure 5.18. Typical spectra of amplitude scintillation in 137-MHz signals received from the HiLat satellite at Hornsund: (a) 24 April 1986 and (b) 28 October 1985. q is the spectral index. (A. W. Wernick *et al.*, *Radio Sci.* **25**, 883, 1990, copyright by the American Geophysical Union.)

Direct measurements

Spatial fluctuations of electron density can be measured *in situ* using satellite-borne probes, though the high velocity of an orbiting satellite limits the structural detail that can be resolved in this manner. In Figure 5.19, which shows measurements of ion (and therefore electron) density made on an orbiting satellite, the fluctuations are as much as 20% of the mean.

In some cases it has been observed that the small-scale irregularities which produce scintillation are located at the edges of large-scale enhancements, and Figure 5.19 is such an example. There are mechanisms (such as the gradient-drift and Kelvin–Helmholtz instabilities) that can cause a large patch to break up at the edges, thereby generating smaller ones, which may break up in turn. By this means the larger structures can progressively break down to give smaller ones in a

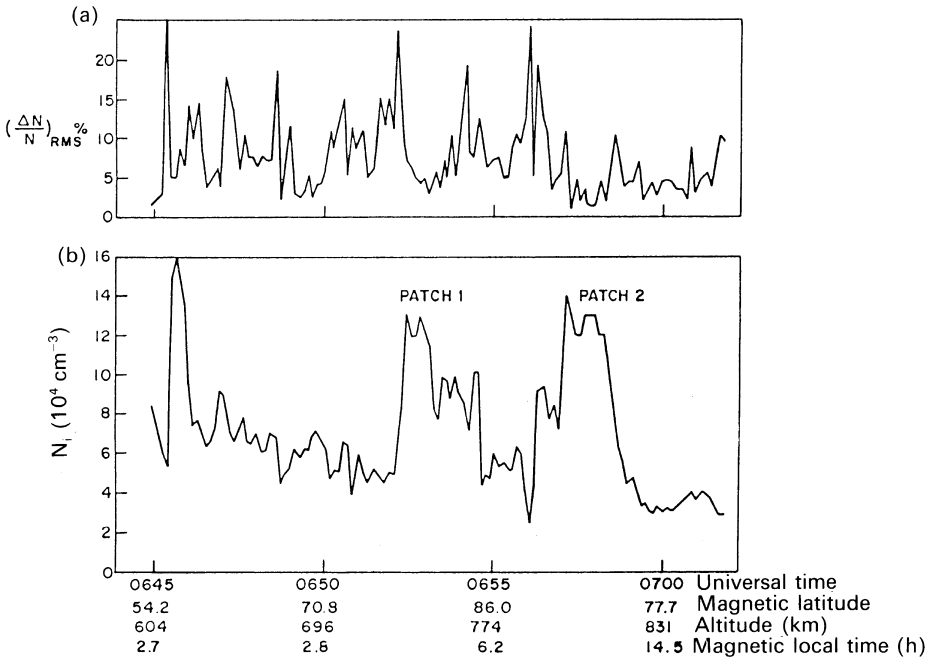

Figure 5.19. (a) Relative irregularity and (b) ion density measured on a satellite crossing the polar cap. In (a) the variation ΔN was taken with respect to a linear least-squares fit to the electron density measured for 3 s; the plotted $\Delta N/N$ therefore refers to irregularities smaller than about 25 km. (After S. Basu *et al.*, *The Effect of the Ionosphere on Communication, Navigation, and Surveillance Systems* (ed. Goodman), p. 599. IES'87, National Technical Information Service, US Government Printing Office, Springfield, Virginia, 1987.)

cascade process. The relationship between large structures in the polar cap and the incidence of radio scintillation has been discussed by Buchau *et al.* (1985).

Modeling

For forecasting purposes, empirical models have been developed to represent the intensity of scintillation at high (and other) latitudes. Scintillation depends on the spatial variation of the electron content, rather than on its actual value (see Section 3.4.5), and varies with parameters such as magnetic latitude and longitude, time of day, season, magnetic activity, and sunspot number. The high-latitude model proposed by Secan *et al.* (1997) is derived from scintillations observed in the 137.67-MHz transmissions from several orbiting satellites (Wideband, HiLat and Polar BEAR) received at stations in Greenland, Norway, Canada, and the USA (Washington State) between 1976 and 1988. Figure 5.20 gives an example showing a quantity called the *irregularity strength parameter* (defined as the power-spectral density of the variation in electron density at the wave number for 1 km, multiplied by the thickness of the irregular region), which is propor-

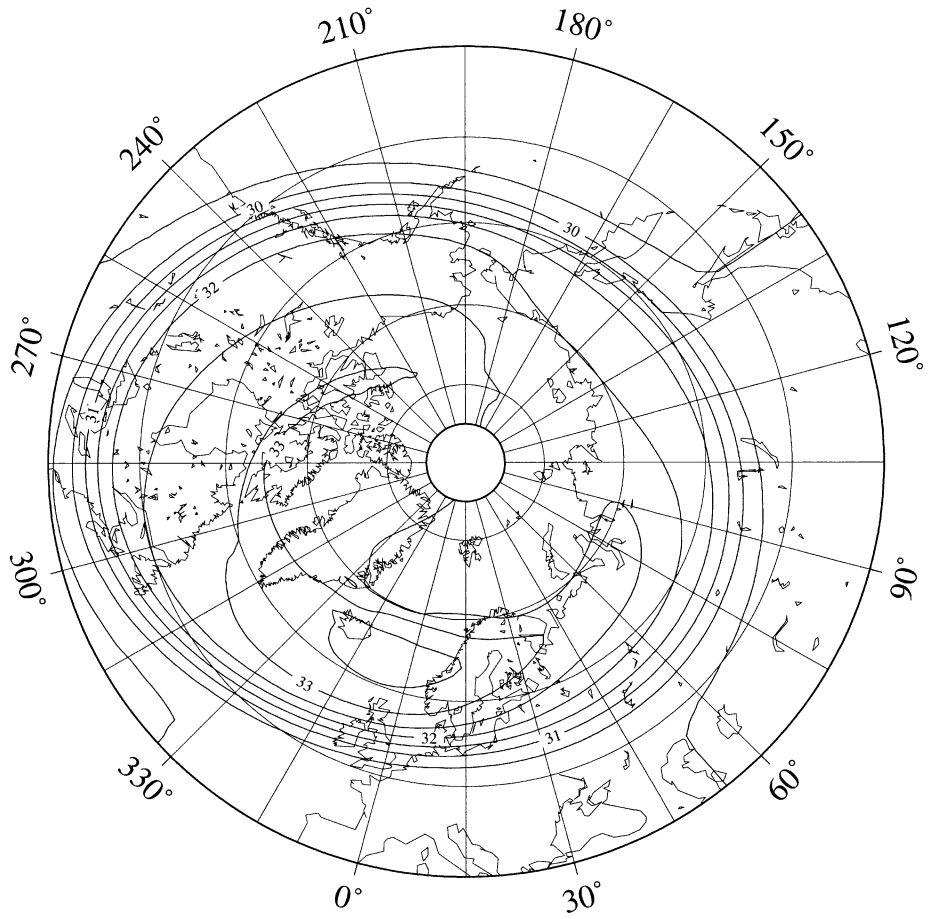

Figure 5.20. Contours of the irregularity parameter C_kL for 2300 UT on 21 July at solar maximum (sunspot number 175) and high geomagnetic activity ($K_p = 6$), from model version 13.04. C_kL is the height integrated power spectrum of irregularities for a periodicity of 1 km, here shown as the logarithm, and is proportional to the variance of the electron content. (J. A. Secan *et al.*, *Radio Sci.* **32**, 1567, 1997, copyright by the American Geophysical Union.)

tional to the variance of the vertical electron content. The calculation of the depth of scintillation is then based on the theory of a phase screen (Section 3.4.5) with an assumed power-law spectrum of intensity. The scintillation index derived depends also on the propagation direction, the radio frequency of the signal, the speed at which the propagation path crosses the plasma irregularities, and assumptions about the height of the effective phase screen and the form of the irregularities.

The data compilation underlying this model revealed several significant features.

(1) The high-latitude scintillation region has a well defined boundary, across which the irregularity strength increases by more than a factor of ten.

(2) The peak of the enhancement associated with the auroral zone lies 2° poleward of the boundary of particle precipitation at midnight, but 14° poleward of it at noon. (The aforsaid precipitation boundary is the equatorward edge of the region where auroral electrons of energies 50 eV to 20 keV are precipitated, as determined by Gussenhoven *et al.* (1983). See also Figure 6.6.)

(3) Equatorward of the scintillation boundary there is a transition region, most evident from 0800 to 1600 magnetic local time, before the irregularity strength assumes the lower values typical of middle latitudes.

(4) The auroral enhancement has maxima near midnight and noon, both of which become more intense with increasing K_p. The night maximum occurs later as K_p increases, and the day maximum occurs later with increasing sunspot number.

(5) The polar cap contains a strong enhancement after noon, and a minimum after midnight. The overall level of irregularity in the polar cap increases with the sunspot number and decreases with increasing K_p.

These features do not show up clearly in Figure 5.20, but are illustrated in Figure 1 of Secan *et al.* (1997), to which the reader is referred for further details of the model and its use.

5.4 The main trough

5.4.1 Introduction

An ionospheric *trough* is a region of depleted ionization, limited in width but extended in the east–west direction, with more intense regions to the north and south. We deal here only with depletions that are observed regularly and appear to be permanent or semi-permanent features of the F region, accepting that they vary in intensity and location. A depletion that is not elongated would be described as a *hole*.

The reader should be warned that the terminology of troughs and holes has been subject to some ambiguity in the literature, as may well happen when phenomena have not yet been fully defined. Most investigations relate to an F-region trough that seems to mark the boundary between the mid-latitude and high-latitude ionospheres. Originally this was called the "mid-latitude" trough, a term that continues to be used. It has also been called the "main" trough, and that term will be prefered here, first to emphasize its importance as the principal trough-like feature of the F region, and second because its occurrence is by no means restricted to middle latitudes. Under a blanket definition of middle and high latitudes, the trough would appear sometimes in one and sometimes in the other, and it is probably more helpful to consider it as the variable boundary between the

high- and middle-latitude regions of the ionosphere, at least on the night side of the Earth. Various other troughs and holes that are wholly within the high-latitude region are observed, and these will be called simply *high-latitude troughs* or *holes*, as the case may be.

Ionospheric troughs are depletions of the heavy ions, principally O^+. They are related to, but not identical to, depletions of light ions (H^+ and He^+) in the topside ionosphere and the protonosphere as far as the equatorial plane. (The inner edge of the main depletion in the plasmasphere is, of course, the plasmapause – Section 2.3.2.)

5.4.2 Observed properties and behavior of the main trough

Observations

The main trough was first observed in the early 1960s by the topside sounder Alouette 1 (Muldrew, 1965; Thomas *et al.*, 1966) as a local depletion of electron density when the satellite crossed the frontier between Canada and the USA. In those early days it was sometimes known as the *Canadian-border effect*. Since then it has been studied from the ground by a variety of techniques, particularly electron-content measurement, incoherent-scatter radar, and by using ionosondes.

An example from Dynamics Explorer 2, showing the variations of electron density and temperature across the northern high-latitude region at the height of the satellite (733–371 km), is shown in Figure 5.21. The main (mid-latitude) trough appears just after 0931 UT near 60° invariant latitude, and two other troughs are seen at higher latitudes. The electron temperature was enhanced in the main trough, and this is typical. The main trough is wider in the example of Figure 5.22, which was derived from ISIS-2 topside ionograms. Here the trough is more than 15° wide, and the complexity of detail in the trough region is indicated. The numbers 1–8 pick out a number of features, namely:

(1) a latitudinal variation in the mid-latitude ionosphere;
(2) the equatorward wall of the trough;
(3) the trough minimum;
(4) the poleward wall of the trough (which is often sharp, as it is here);
(5) an auroral enhancement;
(6) a decline on the poleward side of the auroral oval; and
(7, 8) structure within the polar cap.

Troughs are also observed in the electron content but generally they do not exhibit the sharp gradients or as much detail as those observed by satellite-borne probes or topside sounders. Some examples are given in Figure 5.23. The reason for the different appearance is probably that the electron content is an integral of the electron density rather than the value at one height. Figure 5.23 shows selected

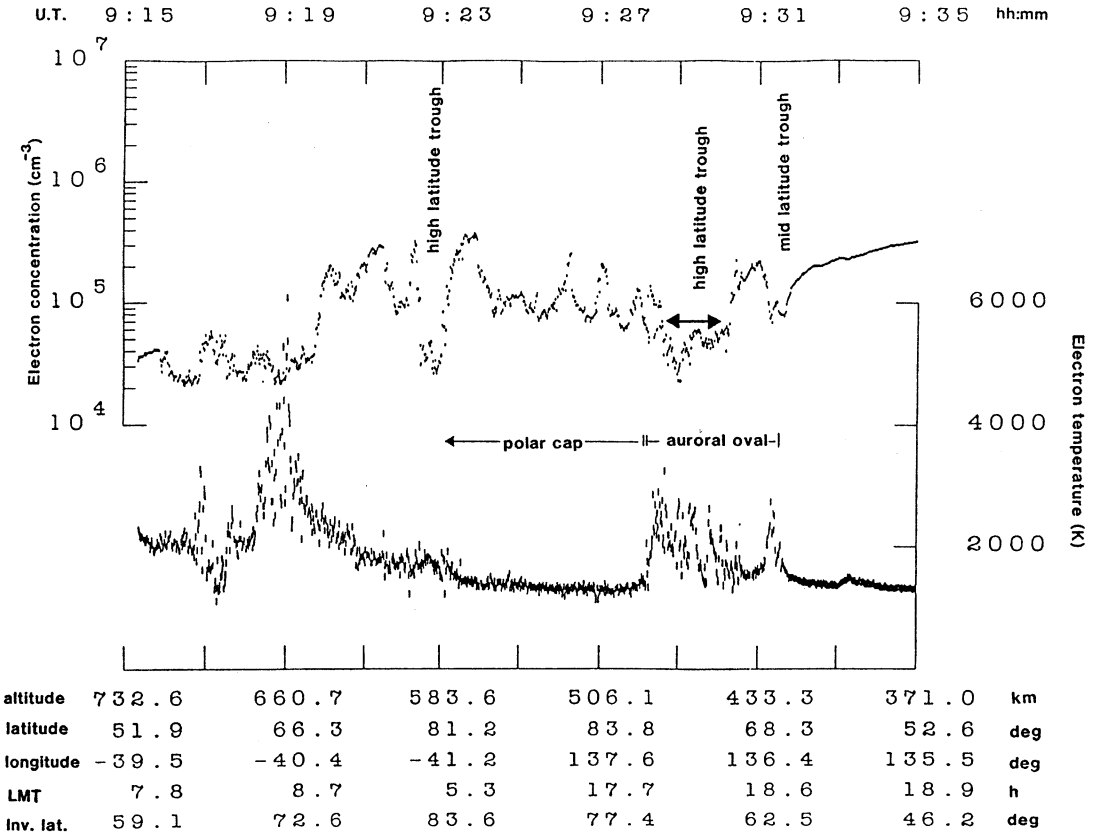

Figure 5.21. Latitude profiles of electron density (left-hand scale) and electron temperature (right-hand scale) measured on the satellite DE-2, 22 November 1981, showing mid-latitude (main) and high-latitude troughs. (Reprinted from A. S. Rodger *et al.*, *J. Atmos. Terr. Phys.* **54**, 1, copyright 1992, with permission from Elsevier Science.)

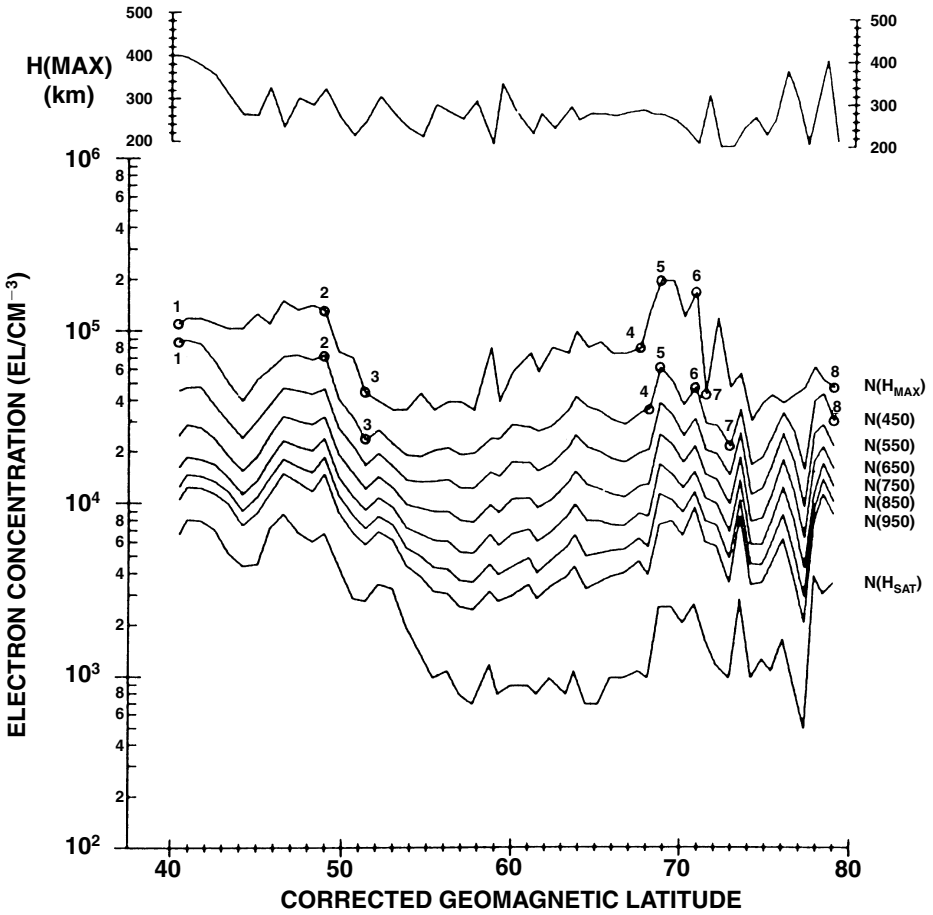

Figure 5.22. Features of the main trough, recorded by the topside sounder ISIS-2 on 18 December 1971. The local time is near midnight. (M. Mendillo and C. C. Chacko, *J. Geophys. Res.* **82**, 5129, 1977, copyright by the American Geophysical Union.)

examples in which the trough is clearly defined. Some troughs are more structured than these, and some have a second minimum.

Figure 5.24 indicates by means of a schematic diagram the structure of the trough as it affects the electron isopleths on the bottom side of the ionosphere near 60° geomagnetic, and in Figure 5.25 we see them both on the topside and on the bottom side obtained by tomographic analysis of electron-content data.

A summary of principal properties (northern hemisphere)

Following Moffett and Quegan (1983), the location and occurrence of the trough (in the northern hemisphere) may be summarized as follows.

- The trough is primarily a night-time phenomenon, extending from dusk to dawn. It has on occasion been observed at all local times.

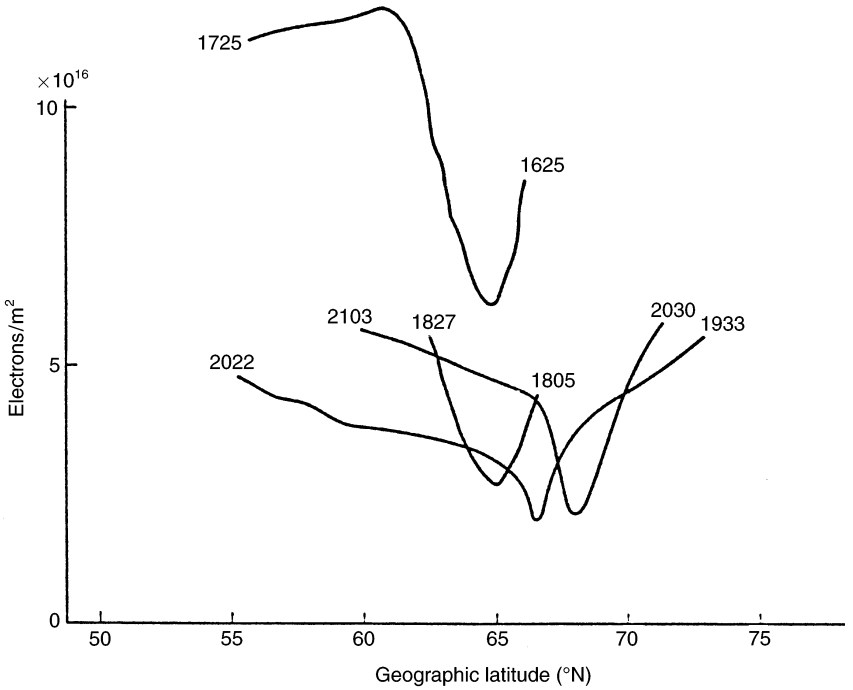

Figure 5.23. Troughs in electron content on four separate occasions when the trough was narrow and well defined. The observations were made in Scandinavia and time is marked in UT. (Reprinted from L. Liszka, *J. Atmos. Terr. Phys.* **29**, 1243, copyright 1967, with permission from Elsevier Science.)

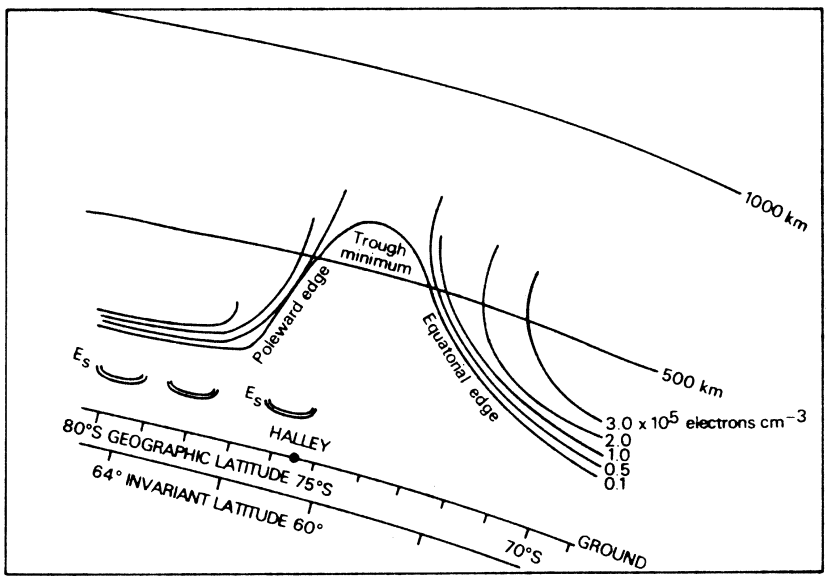

Figure 5.24. A sketch of the trough as it often appears near Halley, Antarctica. (J. R. Dudeney *et al.*, *Radio Sci.* **18**, 927, 1983, copyright by the American Geophysical Union.)

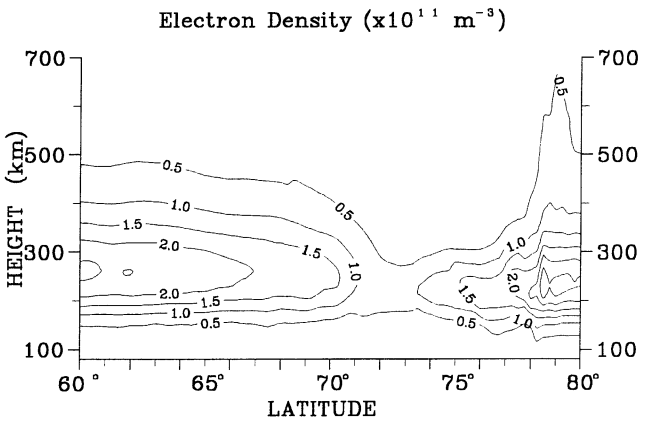

Figure 5.25. The trough as seen by tomography. Results are from the Scandinavian sector, early afternoon, 17 November 1995. Note the narrow upward extension on the poleward side. (L. Kersley, private communication, 1998.)

- It is observed most regularly in the winter and equinoctial seasons. It occurs more rarely in summer, and then only near local midnight.
- The poleward edge of the trough, which is usually sharp, is close to the equatorward edge of the region of diffuse aurora.
- The trough moves to lower latitudes as the night proceeds. Under geomagnetically quiet conditions it can turn back to higher latitudes during the early morning.
- It also moves to lower latitude with increasing geomagnetic activity; solar activity as such appears to have no effect.
- There is no general agreement regarding the depth of the trough or its width, or on how these properties vary with the time of day.

Formulae for variations with time and magnetic activity

Knowledge of the locations both of the trough minimum and of the poleward edge is important for radio communication at high latitudes and for trans-polar paths. The position of the trough minimum as a function of local time and K_p has been expressed by the linear relationship

$$\Lambda_T = \Lambda_0 - aK_p - bt, \tag{5.3}$$

where Λ_T is the invariant latitude of the trough minimum, Λ_0 is its invariant latitude at midnight ($t = 0$) if $K_p = 0$, t is the local time in hours reckoned from midnight (negative before, positive after), and a and b are coefficients. The values of Λ_0, a, and b given in Table 5.3 were derived from independent sets of observations.

These formulae have the merit of simplicity, but they cannot give the whole story because there is no provision for poleward motion in the morning. Halcrow and Nisbet (1977) and Spiro (1978) have derived equations of non-linear form.

Equation (5.3) implies that, at a given latitude, the trough minimum appears

earlier if K_p is higher. The dependence (in h per unit of K_p) is just a/b, or 2.0, 4.2, 3.8, and 1.2, respectively, for the coefficients of Table 5.3.

The increase in the latitude of the trough after about 0700 LT is seen in the electron-content observations (Liszka, 1967) reproduced in Figure 5.26. However, these data are fitted quite well by the formula of Kohnlein and Raitt (shown superimposed) during the hours around midnight. (Liszka's observations were mainly for times of low K_p.) The same data give a K_p dependence of about 2° of latitude for one unit of K_p within the range 0–3 (Figure 5.27), which again agrees with the formula of Kohnlein and Raitt. Note, however, that individual values are spread 2°–3° of latitude about the trend. Rodger *et al.* (1986) have commented that K_p is a poor predictor of the position of the poleward edge of the trough, and this is probably true for all its features except in the statistical sense.

The incoherent-scatter results of Collis and Häggström (1988) were obtained from a review of observations made during a year at sunspot minimum. The troughs were observed during the afternoon and evening hours but none was recorded during the summer period between early April and late August. Their formula gives the strongest variation of latitude with time of day, and significantly higher latitudes during the afternoon than does that of Kohnlein and Raitt. Note that the trough in Figure 5.25 occurred at 72°–74° during the afternoon.

In addition to their formula for the latitude of the minimum, Best *et al.* (1984) also produced expressions in terms of L and for the electron temperature:

$$L(\text{trough minimum}) = 5.4 - 0.5K_p - 0.13t, \tag{5.4}$$

$$L(T_e \text{ maximum}) = 5.2 - 0.4K_p - 0.12t, \tag{5.5}$$

$$T_e(\text{maximum}) = 3250 - 8.06/D_{st}\ \text{K}. \tag{5.6}$$

In Equation (5.6), D_{st} is the magnetic-storm index (Section 2.5.2) in nanoteslas.

Table 5.3. *Coefficients for Equation (5.3)*

Reference	Data source	Λ_0	a (degrees per unit of K_P)	b (degrees h^{-1})	LT for which applicable
Rycroft and Burnell (1970)	Satellite Alouette-1	62.7	1.4	0.7	1900–0500
Kohnlein and Raitt (1977)	Satellite ESRO-4	65.2	2.1	0.5	2000–0700
Best *et al.* (1984)	Satellite Intercosmos 18	64.0	0.5	0.13	Not stated
Collis and Häggström (1988)	EISCAT	62.2	1.6	1.35	1300–0100

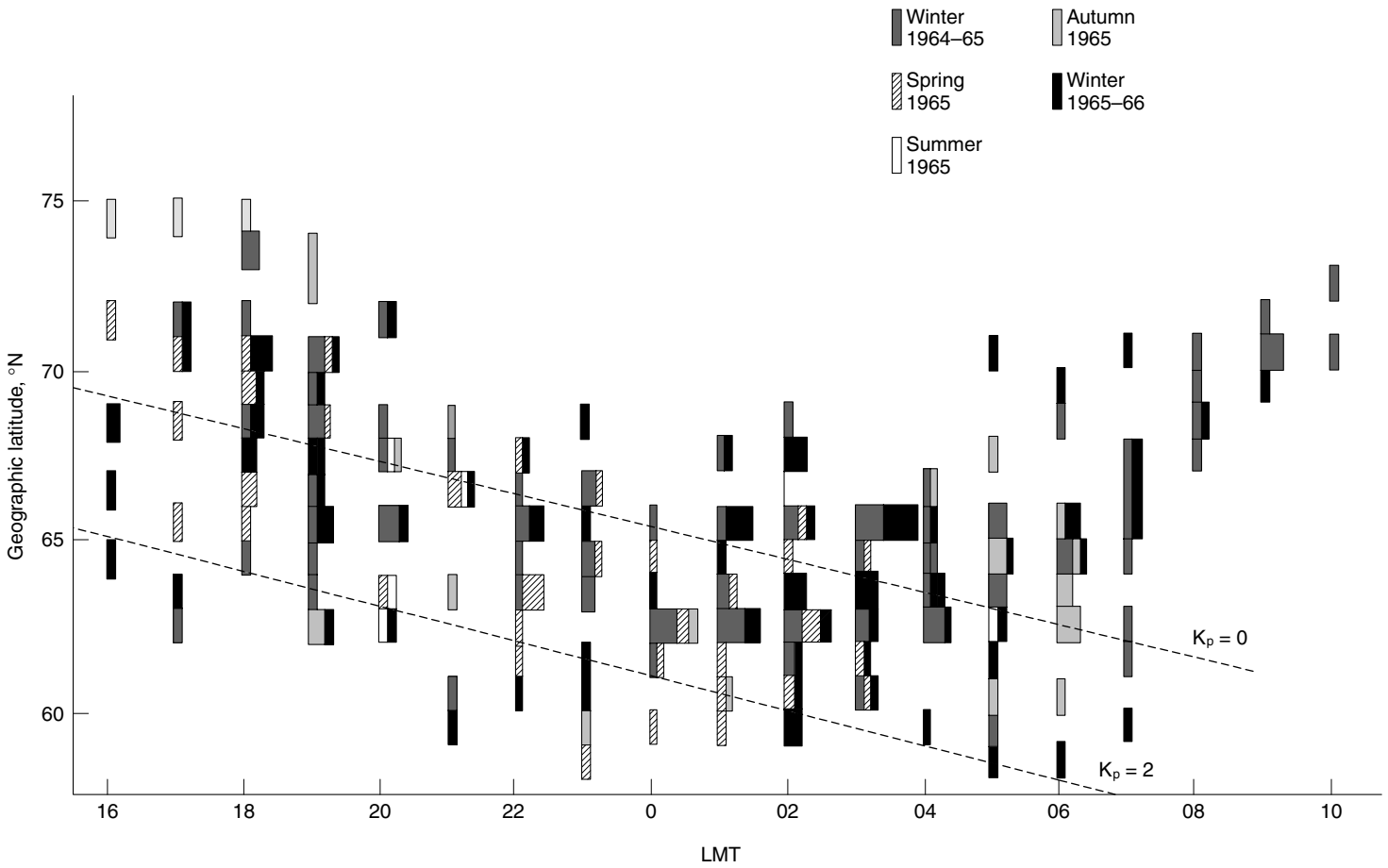

Figure 5.26. Latitude of the trough against local time, from a year's electron-content observations at Kiruna, Sweden. The time is local. (Reprinted from L. Liszka, *J. Atmos. Terr. Phys.* **29**, 1243, copyright 1967, with permission from Elsevier Science.) The trends from the Kohnlein and Raitt formula have been added.

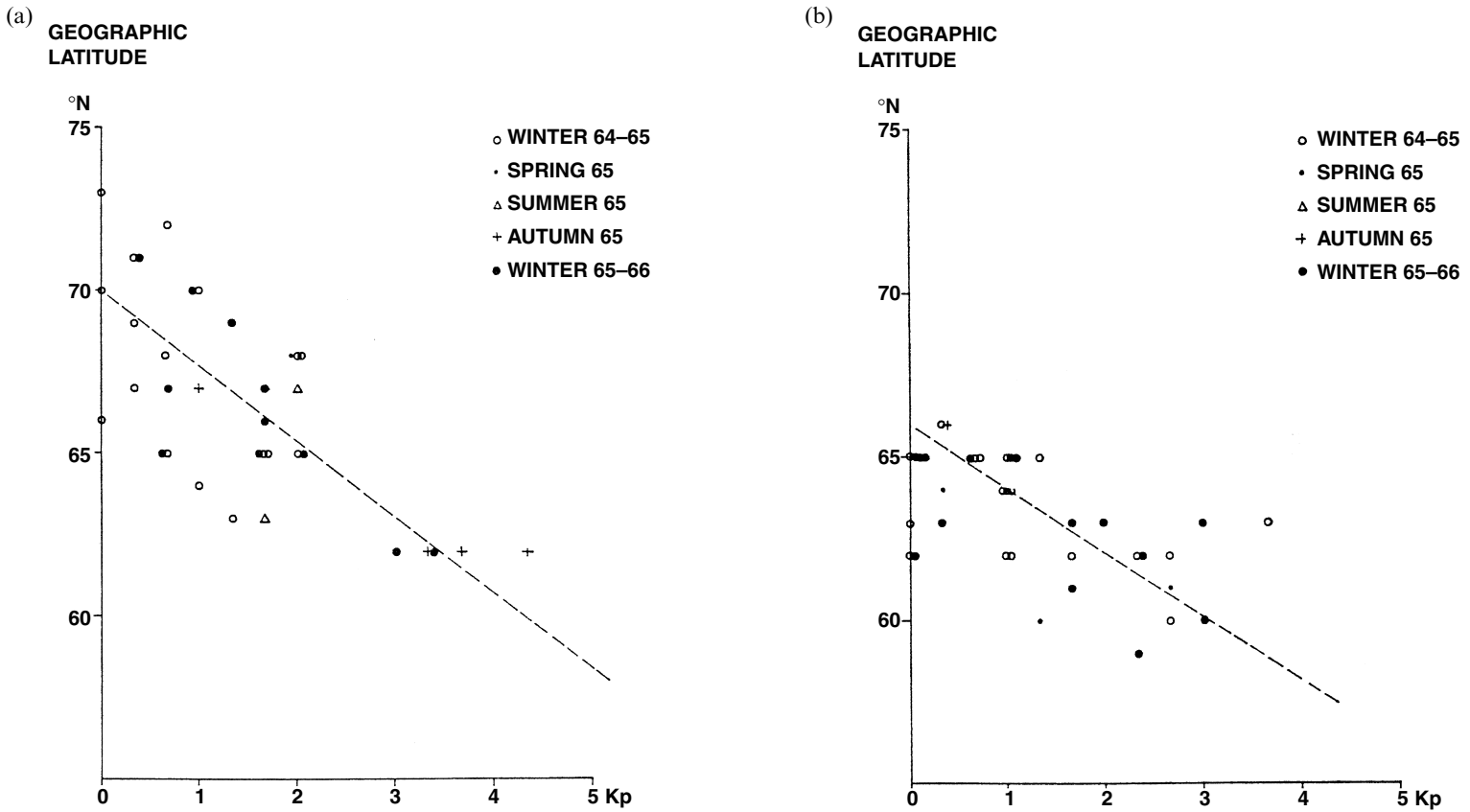

Figure 5.27. Latitude variation of the trough in electron content with the magnetic index K_p: (a) 1900–2000 LMT, and (b) 0300–0400 LMT. (Reprinted from L. Liszka, *J. Atmos. Terr. Phys.* **29**, 1243, copyright 1967, with permission from Elsevier Science.)

The southern hemisphere

The known synoptics of the main trough have been derived mainly from observations in the northern hemisphere. Mallis and Essex (1993) studied the trough in the southern hemisphere as observed in the electron content, and conclude that there are some marked differences between the hemispheres. In the south, troughs are observable in all seasons and at all times of day. They occur less frequently in winter than they do at the equinoxes or in summer, with a relatively high incidence by day. Compared with the north, the southern hemisphere has more troughs by day but fewer by night. It is assumed that these differences are due to hemispheric differences in polar circulation.

5.4.3 The poleward edge of the trough

Introduction

The results in the previous section refer mainly to the minimum of electron density in the trough, but the poleward edge is also a feature of special interest. Valid questions are why the electron density increases again to the poleward side, and why that increase is so sharp. The sharpness of the poleward edge may also be put to use, since it is often the trough feature which is the most easily detected and the most precisely located.

Orientation

The orientation of the trough has been studied using the poleward edge. The equatorward drift of the trough during the night suggests that, at a given time, the trough should not lie exactly along a contour of constant invariant latitude but should be oriented at a small angle to it. This property was investigated in the Antarctic using the Advanced Ionospheric Sounder (AIS) at Halley (76° S, 27° W, $L = 4.2$) by Rodger *et al.* (1986). The AIS can measure the direction of arrival of an ionospheric echo as well as its range. Assuming that the reflection is specular, the position of the perpendicular from the sounder to the edge of the trough can be plotted, and thus the orientation observed.

The results are illustrated in Figure 5.28, which plots the positions of the echoes from troughs observed on 16 occasions. From Halley the perpendicular to the contours of constant invariant latitude is east of south, and close to the direction determined for the period 0000–0159 LT (i.e. line number 4 in panel (c)). Before this time, therefore, the poleward edge is tilted towards lower latitude at later local time (i.e. to the east), and the reverse is true after 0200 LT. The sense of these tilts is consistent with a general equatorward motion during the earlier part of the night and a poleward motion later.

In panel (d), the orientations are mapped into the equatorial plane at $L = 4.2$ and compared with the "teardrop" model of Kavanagh *et al.* (1968) representing

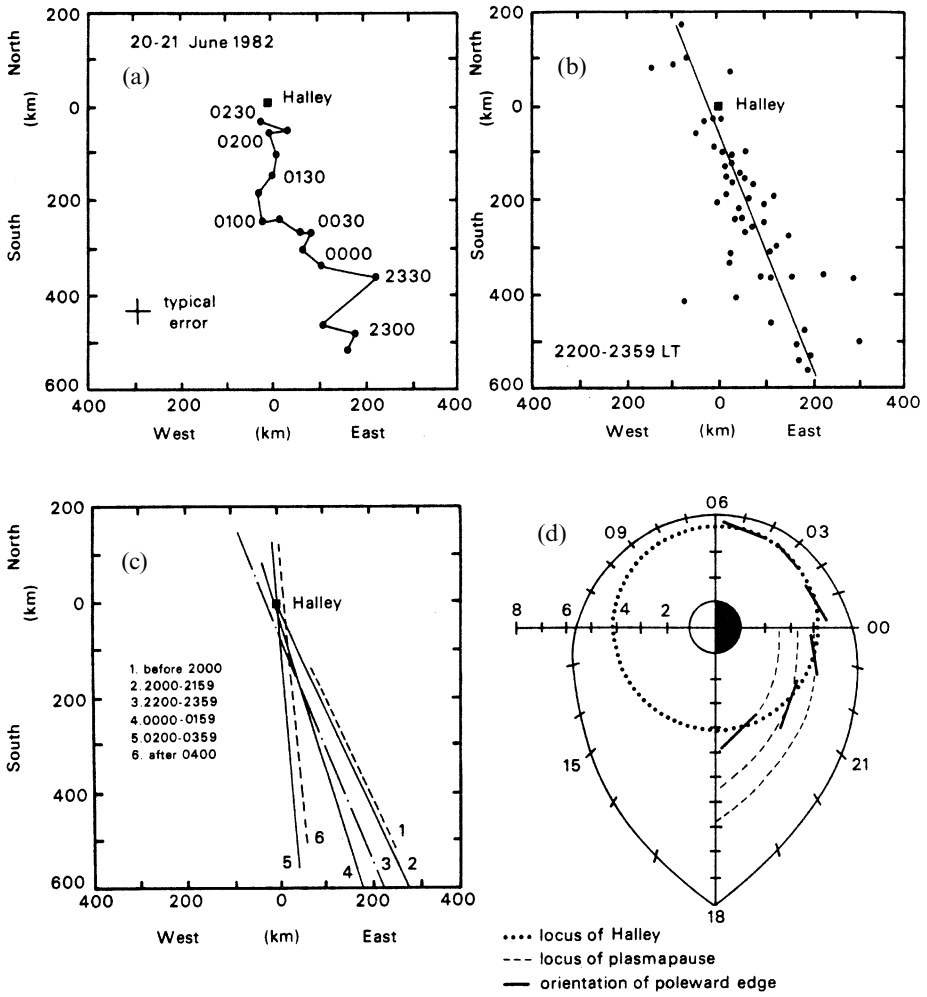

Figure 5.28. On the orientation of the main trough. (a) The location of the poleward edge with respect to Halley on 20–21 June 1982. The time is local. (b) Collection of the poleward edge locations for all observations during 2200–2359 LT, with the best-fitting straight line. (c) The best-fitting straight lines for six 2-h periods. (d) Perpendiculars to the lines in (c) projected to $L = 4.2$ in the equatorial plane and compared with the Kavanagh model of magnetospheric equipotentials. (Reprinted from A. S. Rodger *et al.*, *J. Atmos. Terr. Phys.* **48**, 715, copyright 1986, with permission from Elsevier Science.)

the equipotentials resulting from a simple magnetospheric electric field. It appears that the trough is aligned with the equipotential and, thus, with the direction of plasma drift.

Electron precipitation and the poleward edge

Following the first observations by Bates *et al.* (1973) it has often been noted that the minimum of the trough lies some few degrees equatorward of the edge of the region of auroral precipitation, and it is therefore natural to postulate that auroral

ionization is what causes the electron density to increase on the poleward side of the trough. Supporting evidence comes from particle measurements (Rodger *et al.*, 1986) and from incoherent-scatter radar (Jones *et al.*, 1997). Electron precipitation (at 1 keV) was present on nearly every trough overpass of Dynamics Explorer-2 (DE-2) before 2230 magnetic local time. The radar evidence is of an enhanced electron temperature on the poleward side of the trough. These observations confirm earlier results published by Pike *et al.* (1977).

Later in the night, however, after the passage of the Harang discontinuity (Section 2.5.3), the association was less clear. Two other classes of event were seen, one in which the poleward edge was accompanied by softer electrons (50 eV), and one in which the level of electron precipitation did not alter over the trough. In the DE-2 study, all three types occurred with about the same frequency after midnight. The radar study, also, was unable to establish a clear association with electron precipitation during the second half of the night. The source of the ionization forming the poleward edge is therefore less clear in the post-midnight sector. It is supposed that transport of ionization in the polar circulation is important.

5.4.4 Motions of individual troughs

Most of the studies which produced formulae for the latitude of the trough as functions of the time of day and K_p (Equation (5.3)) were based on observations from (or on signals transmitted from) orbiting satellites. As such, the data consist of a sequence of snapshots taken on different occasions; there is no opportunity to observe any one trough continuously. Therefore these formulae do not neccessarily describe the instantanous motion of the trough. The trough shown in Figure 5.28(a), for example, moved equatorward at 1.3° h^{-1}, a faster drift than would be indicated by any of the formulae except the last of Table 5.3, which, indeed, was based on the tracking of individual examples (by incoherent-scatter radar).

Results from the AIS, tracking the poleward edge from Halley station ($L = 4$), also tend to show relatively high speeds. In the examples in Figure 5.29(a), showing the change of invariant latitude with time, many of the slopes exceed 1° h^{-1}. If the higher speeds were maintained for several hours, these troughs would cover a greater range of latitude than is actually observed. However, it is also significant that, in some cases, the slope flattens out, indicating that the drift is not uniform. The drift speed also varies greatly from one example to another. The examples in Figure 5.29(b), also from Halley, cover the hours 2130–0800 LT overall, though every example extends into the period 0000–0400 LT. The drift speed varies by a factor of ten (from 60 to 600 km h^{-1}), with half the speeds between 100 and 300 km h^{-1} and the median at 200 km h^{-1} (1.8° h^{-1}).

The examples in Figure 5.29(c) are from electron-content measurements from a site in the auroral zone. (The local time is UT − 1 h.) At this higher latitude the trough is seen during the afternoon, but note that the locations and the speeds again agree with the formula of Collis and Häggström (C + H) rather than with

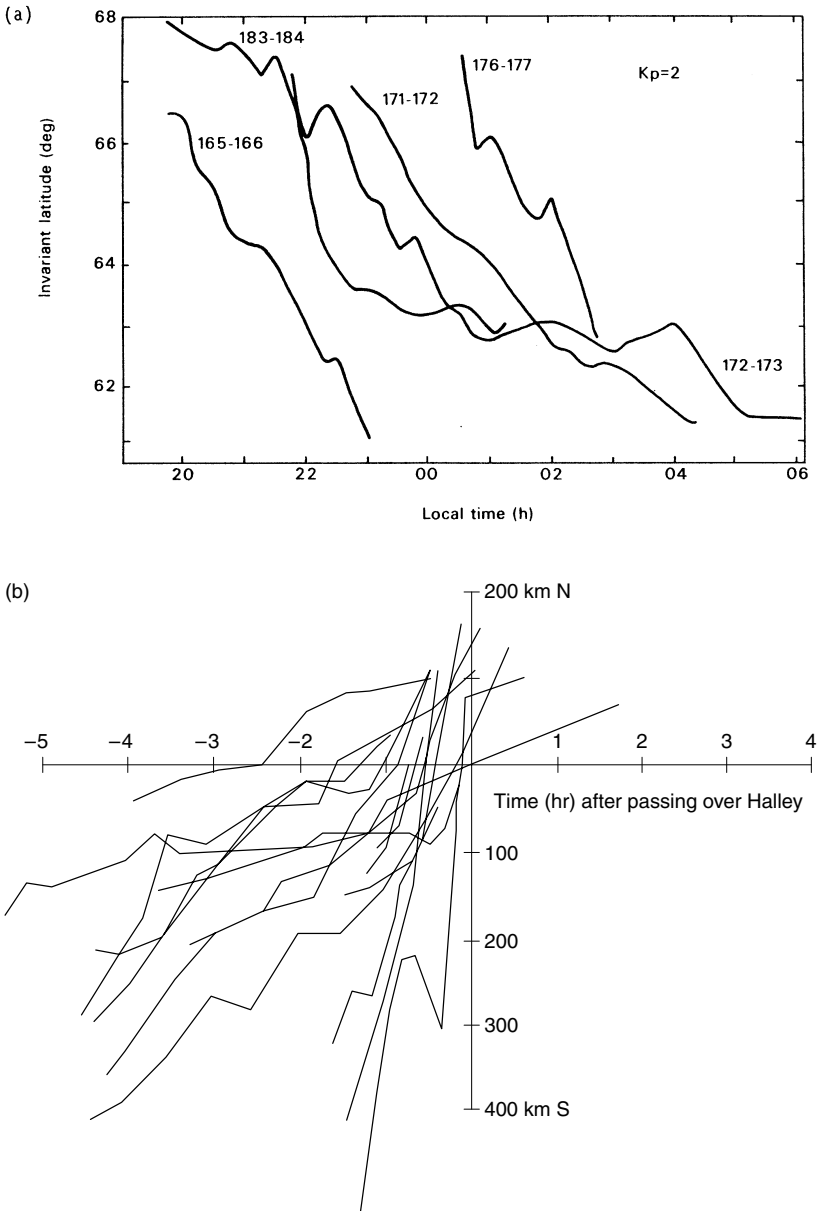

Figure 5.29. The latitudinal drift of the main trough. (a) The poleward edge observed by the Halley Advanced Ionospheric Sounder for five nights of 1982. In each case $K_p = 2$. (Reprinted from A. S. Rodger *et al.*, *J. Atmos. Terr. Phys.* **48**, 715, copyright 1986, with permission from Elsevier Science.) (b) A collection of Halley troughs from 1982–1983, showing the variability of the speed of equatorward drift. (Time is counted from the appearance of a weak precipitation event associated with the poleward edge.) (W. G. Howarth and J. K. Hargreaves, private communication.) (c) Trough minima from electron-content measurements in the auroral zone in Scandinavia. Values of K_p are marked and the formulae of Kohnlein and Raitt, and of Collis and Haggestrom have been superimposed. (Reprinted from J. K. Hargreaves and C. J. Burns, *J. Atmos. Terr. Phys.* **58**, 1449, Copyright 1996, with permission from Elsevier Science.)

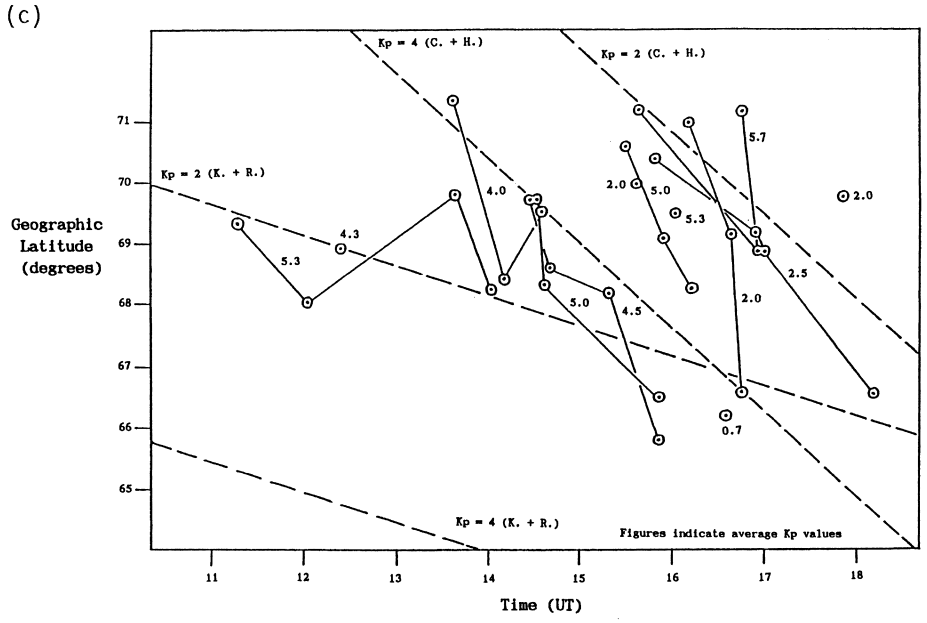

Figure 5.29. (*cont.*)

that of Kohnlein and Raitt (K + R). These troughs would not link up with those shown in Figure 5.29(a) if they continued to move equatorward at the same speed. Thus, the evidence indicates that, although formulae based on satellite data may express the latitude at which the trough is likely to be seen, individual troughs move considerably faster than those formulae would indicate.

One explanation (Rodger *et al.*, 1986) is based on the effect of substorms, which on some occasions are seen to be related to a partial filling of the trough from the poleward side. Figure 5.30 illustrates the point, showing how the polar edge steepened between two successive orbits of the satellite DE-2, a substorm having commenced in the interim. This filling was most likely due to enhanced particle precipitation due to the substorm. This is a new factor, not included in the assumptions of Equation (5.3), but it is not clear whether this is the whole explanation.

5.4.5 Mechanisms and models

The main trough caused by plasma decay

Since the main trough lies between the mid- and high-latitude ionospheres, one may reasonably expect that its cause has some connection with the different circulation patterns in those two regions. Various attempts to predict the position of the trough have been made by modeling the ionosphere mathematically (Moffett and Quegan, 1983). These models represent the high-latitude convection in a

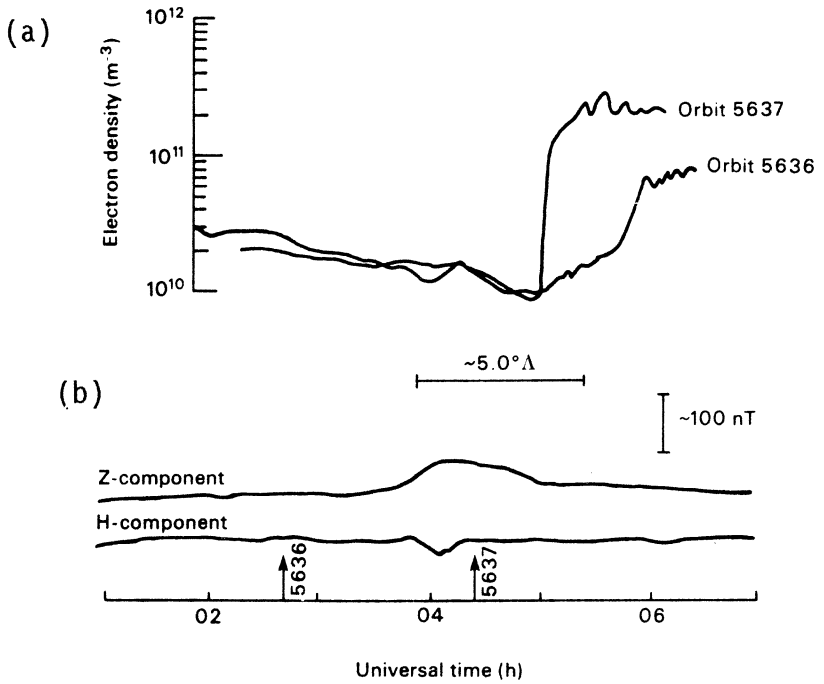

Figure 5.30. (a) Two consecutive passes of DE-2 near Halley on 14 August 1982, showing a steepening of the poleward edge. (b) The Halley magnetometer indicated that a substorm occurred between those two orbits. (Reprinted from A. S. Rodger *et al.*, *J. Atmos. Terr. Phys.* **48**, 715, copyright 1986, with permission from Elsevier Science.)

steady state and, although they might not include all the physical processes that could be relevant, they do predict a main trough in about the right place. The basic cause is that there are some convection paths (e.g. path 5 in Figure 5.1(b)) which do not encounter a production region for several hours, a time long enough for the plasma density to decay to a low value. Measurements by incoherent-scatter radar (Collis and Haggstrom, 1988) support this theory, showing that the trough minimum generally lies in a zone where the plasma flow (with respect to the Earth) is strongly westward. Such a flow tends to offest the Earth's rotation and hence prolong the time for which the plasma remains in a dark region.

One possible complication is that a steady-state pattern of convection is unlikely to continue for very long, due to the constant variations in the solar wind which drives the polar convection. While ionization decay is now accepted as the essential cause of the main trough, we are some way from being able to predict details of the trough for any given day.

Other mechanisms

Rodger *et al.* (1992) reviewed all the mechanisms that could create, or help to create, ionization troughs, and concluded that the difference in velocity between

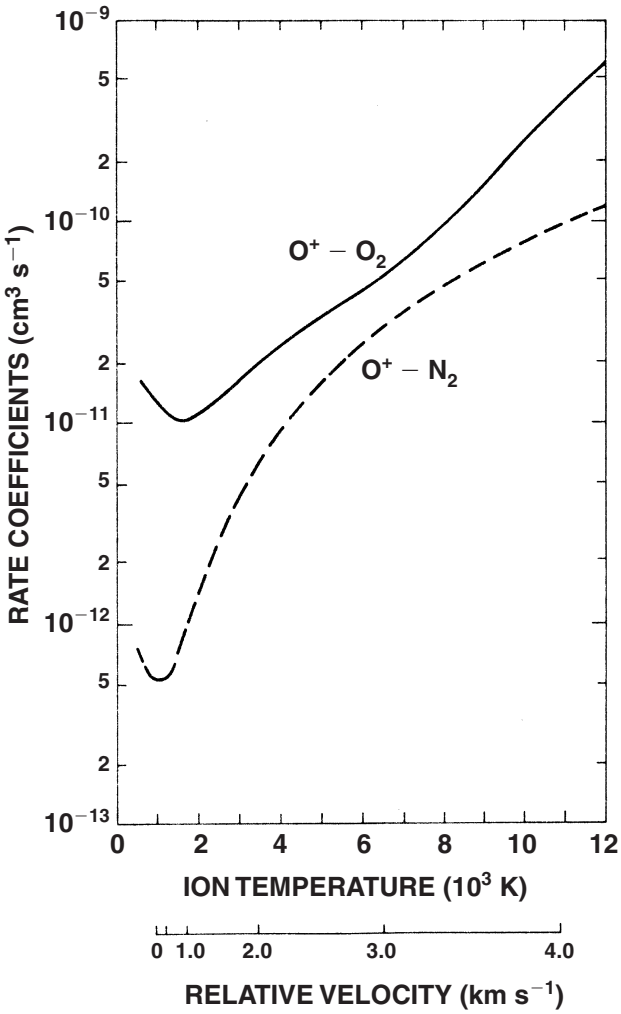

Figure 5.31. Temperature dependences of recombination reactions in the F region. The relative velocity of ions and neutral species is shown on the second scale. (Reprinted from A. S. Rodger *et al.*, *J. Atmos. Terr. Phys.* **54**, 1, copyright 1992, with permission from Elsevier Science.)

ions and neutral particles is likely to be an important factor. The rate coefficients k_1 and k_2 in the expression for the recombination coefficient

$$\beta = k_1[N_2] + k_2[O_2] \tag{5.7}$$

are temperature dependent, as shown in Figure 5.31, and a relative drift between the ions and the neutral species heats the gas. Figure 5.31 shows the relative velocity as a second abscissa scale. The heating increases the rate of loss by recombination and causes an upward flow of plasma that also depletes the F region. It is argued, therefore, that plasma depletion is expected in regions heated by high differences in speed between ions and neutral particles.

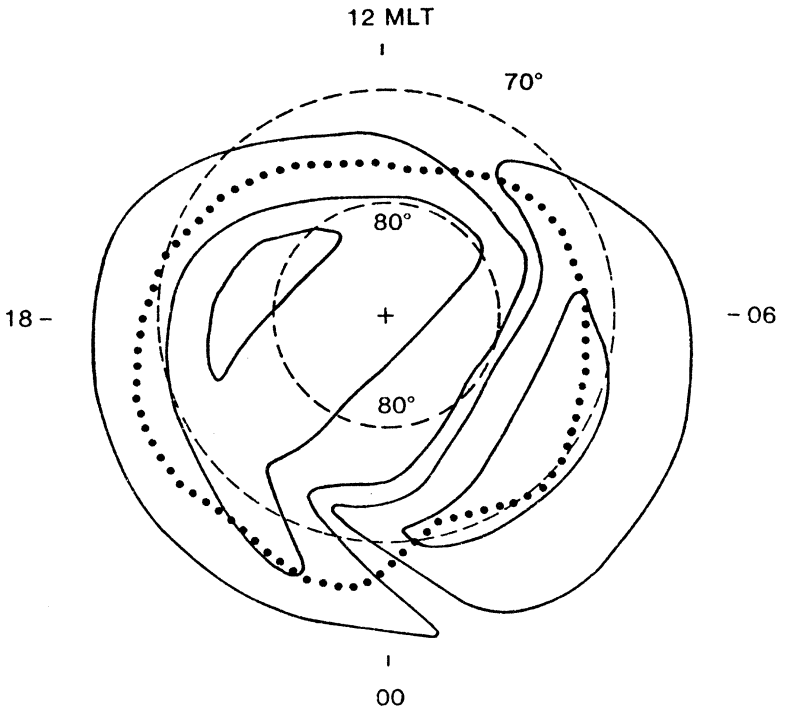

Figure 5.32. The average location of the high-latitude trough determined from passes of the satellite OGO-6 (dotted line), plotted over an electric-field pattern (solid lines). (Reprinted from A. S. Rodger *et al.*, *J. Atmos. Terr. Phys.* **54**, 1, copyright 1992, with permission from Elsevier Science.)

5.5 Troughs and holes at high latitude

Depletions occurring poleward of the main trough – that is, within the auroral oval and polar cap – have been observed by incoherent-scatter radar and in satellite passes, but in general they have not been so intensively studied as the main trough. Rodger *et al.* (1992) have summarized the principal features of these troughs as follows.

- *High-latitude troughs* are between 5° and 9° wide, with a poleward edge between 67° and 71° magnetic latitude and an equatorward edge between 61° and 67°. (Note that this overlaps with the position of the main trough in the afternoon sector.)
- They last for 4–8 h, moving to higher latitude towards the end of the period.
- Their equatorward edge moves equatorward with increasing K_p, and there is some evidence that the trough forms earlier when K_p is larger.
- They are often associated with a reversal of the convection (as a function of latitude) in the morning sector, but in the evening are on the equatorward side of the reversal. Figure 5.32 illustrates this point.

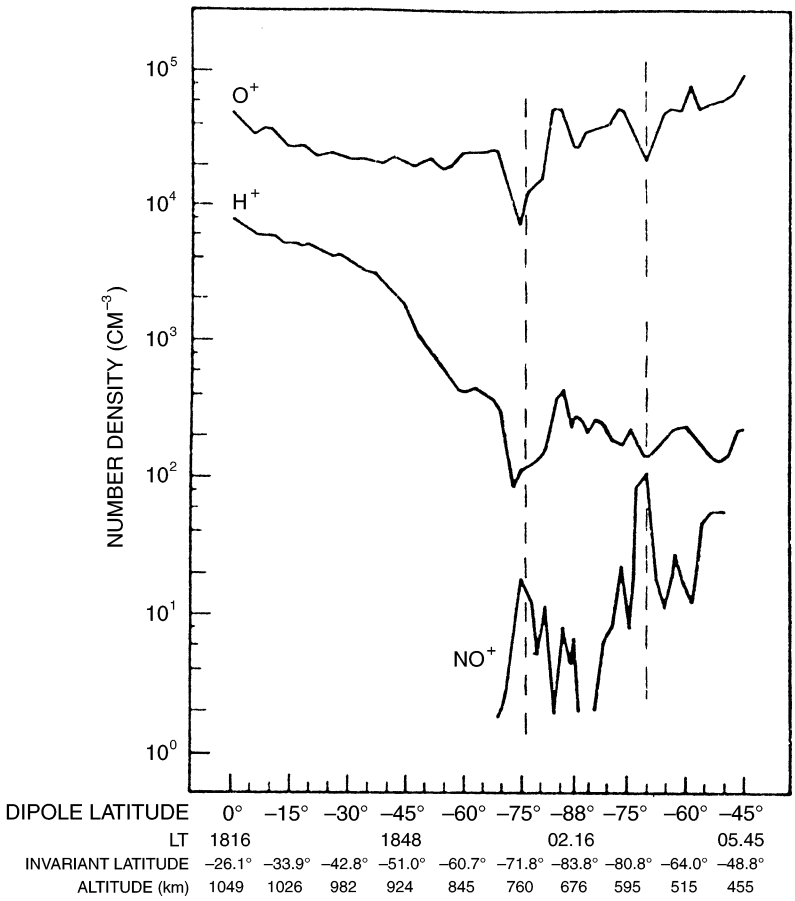

Figure 5.33. High-latitude troughs in O^+ and H^+ at 70°–75° north, from OGO-6, 18 March 1970, 1830–1854 $K_p = 2^+$. There is an enhancement in concentration of the molecular species NO^+. (Reprinted from J. M. Grebowsky *et al.*, *Planet. Space Sci.* **31**, 99, copyright 1983, with permission from Elsevier Science.)

- The ion temperature (T_i) and the electric field are usually increased within the trough but the electron temperature is not usually affected.
- There are relationships between T_i and the field-aligned plasma velocity.
- The atomic ions (H^+, O^+, and N^+) are reduced in concentration, but concentrations of molecular species (NO^+ and O_2^+) are increased.

Figure 5.33 shows further examples of high-latitude troughs in terms of the ion densities; note the enhancements in concentration of NO^+.

The *polar hole* is recognized as a distinct feature. It is a long-lived depletion observed in years of low solar activity during winter in the Antarctic polar cap (Brinton *et al.*, 1978), occurring shortly after midnight at magnetic latitudes near 80°. The electron density (at 300 km) is as low as $(1–3) \times 10^2$ cm^{-3}, compared with up to 10^5 cm^{-3} elsewhere in the polar cap. The hole appears sporadically at the

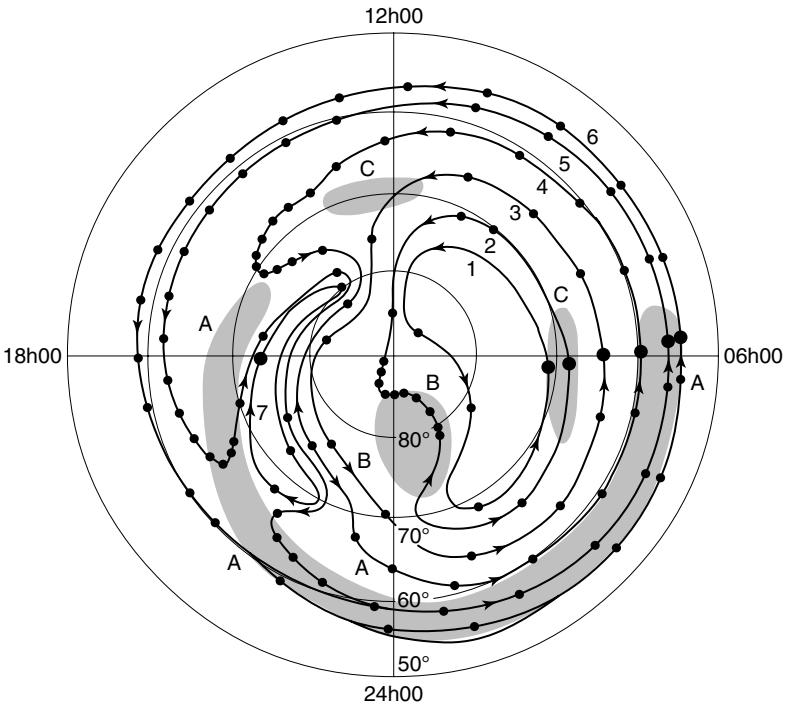

Figure 5.34. A summary of F-region depletions under steady geophysical conditions when the cross-tail electric field is small. The solar terminator is along the line 1800–0600. A, main trough; B, polar hole. C, region of significant frictional heating of ions and neutral species. The features are superposed on the polar convection pattern of Figure 5.1(b). (Reprinted from A. S. Rodger *et al.*, *J. Atmos. Terr. Phys.* **54**, 1, copyright 1992, with permission from Elsevier Science.)

equinoxes and hardly ever in summer. The seasonal variation can be explained by invoking the movement of the solar terminator, which ensures that the relevant region is dark in winter but illuminated in summer. The electron temperature is reduced in the polar hole and the ion speeds are low. Concentrations of molecular species are not enhanced there. For reasons that remain unknown, the polar hole has not been observed in the Arctic.

It must be appreciated that it is not unusual for the high-latitude ionosphere to be irregular where it is not illuminated by the Sun. We have drawn attention in Section 5.3.2 to the phenomena of patches and blobs in the high-latitude ionosphere, where the emphasis is on the enhancements. A study of the depletions should be complementary to this, and it might not always be clear whether it is the enhancement or the depletion which is abnormal. In some cases the structure may actually comprise both – that is, the mechanism may remove ionization from one place and concentrate it elsewhere.

Figure 5.34 summarizes the location of high-latitude depletions (as well as the main trough). Table 5.4 describes the various features.

Table 5.4. *Characteristics of features in Figure 5.34*

Trough type	V_i	T_e	T_i	Composition	Comment
A. Stagnation trough	Low	High	Normal	Normal	Protonospheric maintenance affects equatorward edge; high T_e by virtue of conduction of heat from high altitudes
B. Polar hole	Low	Low	Presumably low, although no measurements have been made	Normal	Enhancements of He^+ and H^+ concentrations in the topside
C. High electric field in rest frame of neutral species	High >1 km s^{-1}	??	High and anisotropic	NO^+ rich	Joule heating and outflow of ions can be significant; often occurs in regions of high electron precipitation, and thus T_e can be elevated

The reader is referred to the review paper by Rodger *et al.* (1992) for further details and for discussion of other high-latitude depletions of the F region.

5.6 Summary and implications

In radio propagation the F region principally affects systems operating at the higher frequencies, specifically in the HF, VHF, and UHF bands. Effects can be major even when the F region is undisturbed, especially during the winter season when electron densities tend to become very small during the long polar night. During geomagnetic storms and substorms additional effects appear. The precipitation of energetic charged particles increases, whereupon circuits operating in these bands may be seriously degraded.

The main ionospheric trough, a region of depleted electron density just equatorward of the auroral oval, depresses HF operating frequencies when the reflection or control points come within its boundaries. The main trough is a semi-permanent feature at the transition between the mid-latitude and the high-latitude ionospheres, occurring mainly at night and more strongly in winter than in summer in the northern hemisphere. The incidence is somewhat different in the southern hemisphere.

When energetic electrons and protons precipitate into the auroral F region they produce field-aligned irregularities of various sizes, which may deviate and scatter HF to UHF signals incident on them. Backscatter may be produced by the component of irregularity having a wavelength equal to half the radio wavelength when the signal is propagating in a direction essentially normal to the geomagnetic field-lines. The geometry is such that HF scattering is most likely to occur when signals propagate from temperate latitudes towards and into the auroral oval. HF radars operated for research purposes make use of this backscatter to study the structure and dynamics of the polar ionosphere. Over-the-horizon HF radars experience system degradation by field-aligned irregularities, and satellite-to-earth VHF and UHF signals suffer scintillation phenomena causing a rapid and sometimes severe fading of amplitude and irregular fluctuations of phase.

In the polar ionosphere, by which we mean that part poleward of the auroral zone, the particle precipitation is generally not as intense as that into the oval. Nevertheless, some major F-region irregularities do occur. The dominant features, known as arcs or patches, are enhancements of F-region plasma density that probably originate not locally but in the ionosphere at lower latitude, and then drift over the polar cap under the control of the electric field between the dusk and dawn sides of the polar cap. There is now a substantial body of knowledge about these structures, though it is not yet sufficient for prediction purposes.

A detailed description of the effects of the high-latitude F region on the propagation of radio signals over the whole spectrum from MF to UHF is given in Chapters 8 and 9.

5.7 References and bibliography

5.1 Circulation of the high-latitude ionosphere

Boyle, C. B., Reiff, P. H., and Hairston, M. R. (1997). Empirical polar cap potentials. *J. Geophys. Res.* **102**, 111.

Cowley, S. W. and Lockwood, M. (1997) Excitation and decay of solar wind-driven flows in the magnetosphere-ionosphere system. *Ann. Geophysicae*. **10**, 103.

Dudeney, J. R., Rodger, A. S., Pinnock, M., Ruohoniemi, J. M., Baker K. B., and Greenwald, R. A. (1991) Studies of conjugate plasma convection in the vicinity of the Harang discontinuity. *J. Atmos. Terr. Phys.* **53**, 249.

Hairston, M. R. and Heelis, R. A. (1995) Response time of the polar ionospheric convection pattern to changes in the north-south direction of the IMF. *Geophys. Res. Lett.* **22**, 631.

Jayachandran, P. T. and MacDougall, J. W. (1999) Seasonal and B_y effect on the polar cap convection. *Geophys. Res. Lett.* **26**, 975.

Kelley, M. C. (1989) Section 6.2. In *The Earth's Ionosphere*. Academic Press, New York.

Lu, G. and 20 others. (1994) Interhemispheric asymmetry of the high-latitude ionospheric convection pattern. *J. Geophys. Res*. **99**, 6491.

Rich, F. J. and Hairston, M. (1994) Large-scale convection patterns observed by DMSP. *J. Geophys. Res.* **99**, 3827.

Ruohoniemi, J. M. and Greenwald, R. A. (1996) Statistical patterns of high-latitude convection obtained from Goose Bay HF radar observations. *J. Geophys. Res.* **101**, 21 743.

Todd, H., Bromage, B. J. I., Cowley, S. W. H., Lockwood, M., van Eyken, A. P., and Willis, D. M. (1986) EISCAT observations of rapid flow in the high latitude dayside ionosphere. *Geophys. Res. Lett.* **13**, 909.

Willis, D. M., Lockwood, M., Cowley, S. W. H., van Eyken, A. P., Bromage, B. J. I., Rishbeth, H., Smith, P. R., and Crothers, S. R. (1986) A survey of simultaneous observations of the high-latitude ionosphere and interplanetary magnetic field with EISCAT and AMPTE UKS. *J. Atmos. Terr. Phys.* **48**, 987.

5.2 Behaviour of the F region at high latitude

Farmer, A. D., Crothers, S. R., and Davda, V. N. (1990) The winter anomaly at Tromsø. *J. Atmos. Terr. Phys.* **52**, 561.

Muldrew, D. B. and Vickrey, J. F. (1982) High-latitude F region enhancements observed simultaneously with ISIS 1 and the Chatanika radar. *J. Geophys. Res.* **87**, 8263.

Raitt, W. J. and Schunk, R. W. (1983) Composition and characteristics of the polar wind. In *Energetic Ion Composition in the Earth's Magnetosphere* (ed. R. G. Johnson), p. 99. Terra Scientific Publishing, Tokyo.

Robinson, R. M., Tsunoda, R. T., Vickrey, J. F., and Guerin, L. (1985) Sources of F-region ionization enhancements in the night-time auroral zone. *J. Geophys. Res.* **90**, 7533.

Walker, I. K., Moen, J., Mitchell, C. N., Kersley, L., and Sandholt, P. E. (1998) Ionospheric effects of magnetopause reconnection observed by ionospheric tomography. *Geophys. Res. Lett.* **25**, 293.

Whitteker, J. H., Shepherd, G. G., Anger, C. D., Burrows, J. R., Wallis, D. D., Klumpar, D. M., and Walker, J. R. (1978) The winter polar ionosphere. *J. Geophys. Res.* **83**, 1503.

5.3 Irregularities of the F region at high latitude

Aarons, J. (1982) Global morphology of ionospheric scintillations. *Proc IEEE* **70**, 360.

Anderson, D. N., Buchau, J., and Heelis, R. A. (1988) Origin of density enhancements in the winter polar-cap ionosphere. *Radio Sci.* **23**, 513.

Buchau, J., Reinish, B. W., Weber, E. J., and Moore, J. F. (1983) Structure and dynamics of the winter polar cap F region. *Radio Sci.* **18**, 995.

Buchau, J., Weber, E. J., Anderson, D. N., Carlson, H. C., Moore, J. G., Reinisch, B. W., and Livingston, R. C. (1985) Ionospheric structures in the polar cap: their origin and relation to 250 MHz scintillation. *Radio Sci.* **20**, 325.

Burns, C. J. and Hargreaves, J. K. (1996) The occurrence and properties of large-scale electron-density structures in the auroral F region. *J. Atmos. Terr. Phys.* **58**, 217.

Carlson, H. C., Wickwar, V. B., Weber, E. J., Buchau, J., Moore, J. G., and Whiting, W (1984). Plasma characteristics of polar cap F-layer arcs. *Geophys. Res. Lett.* **11**, 895.

de la Beaujardière, O. and Heelis, R. A. (1984) Velocity spike at the poleward edge of the auroral zone. *J. Geophys. Res.* **89**, 1627.

Gussenhoven, M. S., Hardy, D. A., and Heinemann, N. (1983) Systematics of the equatorward diffuse auroral boundary. *J. Geophys. Res.* **88**, 5692.

Hargreaves, J. K., Burns, C. J., and Kirkwood, S. C. (1985a) EISCAT studies of F-region irregularities using beam scanning. *Radio Sci.* **20**, 745.

Hargreaves, J. K., Burns, C. J., and Kirkwood, S. C. (1985b) Irregular structures in the high-latitude F-region observed using the EISCAT incoherent scatter radar. *Proc. AGARD Conference 382* (Fairbanks, Alaska) p. 6.2-1.

Kelley, M. C., Baker, K. D., Ulwick, J. C., Rino, C. L., and Baron, M. J. (1980) Simultaneous rocket probe, scintillation and incoherent scatter observations of irregularities in the auroral zone ionosphere. *Radio Sci.* **15**, 491.

Lockwood, M. and Carlson, H. C. (1992) Production of polar cap electron density patches by transient magnetopause reconnection. *Geophys. Res. Lett.* **19**, 1731.

Muldrew, D. B. and Vickrey, J. F. (1982) High-latitude F region irregularities observed simultaneously with ISIS 1 and the Chatanika radar. *J. Geophys. Res.* **87**, 8263.

Radio Science (1994) Special section on high-latitude structures. *Radio Sci.* **29**, 155–315.

Rino, C. L. (1978) Evidence for sheetlike auroral ionospheric irregularities. *Geophys. Res. Lett.* **5**, 1039.

Rino, C. L., Livingston, R. C., Tsunoda, R. T., Robinson, R. M., Vickrey, J. F., Senior, C., Cousins, M. D., and Owen, J. (1983) Recent studies of the structure and morphology of auroral-zone F-region irregularities. *Radio Sci.* **18**, 1167.

Robinson, R. M., Tsunoda, R. T., Vickrey, J. F., and Guerin, L. (1985) Sources of F-region ionization enhancements in the night-time auroral zone. *J. Geophys. Res.* **90**, 7533.

Secan, J. A., Bussey, R. M., Fremouw, E. J., and Basu, S. (1997) High-latitude upgrade to the Wideband ionospheric scintillation model. *Radio Sci.* **32**, 1567.

Sojka, J. J., Bowline, M. D., Schunk, R. W., Decker, D. T., Valladares, C. E., Sheehan, R., Anderson, D. N., and Heelis, R. A. (1993) Modelling polar cap F region patches using time varying convection. *Geophys. Res. Lett.* **20**, 1783.

Sojka, J. J., Bowline, M. D., and Schunk, R. W. (1994) Patches in the polar ionosphere: UT and seasonal dependence. *J. Geophys. Res.* **99**, 14959.

Tsunoda, R. T. (1988) High-latitude F region irregularities: a review and synthesis. *Rev. Geophys.* **26**, 719.

Vickrey, J. F., Rino, L. C. and Potemra, T. A. (1980) Chatanika/TRIAD observations of unstable ionization enhancements in the auroral F-region. *Geophys. Res. Lett.* **7**, 789.

Weber, E. J. and Buchau, J. (1981) Polar cap F layer auroras. *Geophys. Res. Lett.* **8**, 125.

Weber, E. J. and Buchau, J. (1985) Observations of plasma structure and transport at high latitudes. *The Polar Cusp* (eds. Holtet and Egeland) p. 279. Reidel, Hingham, Massachusetts.

Weber, E. J., Buchau, J., Moore, J. G., Sharber, J. R., Livingston, R. C. ,Winningham, J. D., and Reinisch, B. W. (1984) F layer ionization patches in the polar cap. *J. Geophys. Res.* **89**, 1683.

Weber, E. J., Klobuchar, J. A., Buchau, J., Carlson, H. C., Livingston, R. C., de la Beaujardière, O., McCready, M., Moore, J. G., and Bishop, G. J. (1986) Polar cap F-layer patches: structure and dynamics. *J. Geophys. Res.* **91**, 12121.

Yeh, K. C. and Liu, C. H. (1982) Radio wave scintillation in the ionosphere. *Proc. IEEE* **70**, 324.

5.4 The main trough

Bates, H. F., Belon, A. E., and Hunsucker, R. D. (1973) Aurora and the poleward edge of the main ionospheric trough. *J. Geophys. Res.* **78**, 648.

Best, A., Best, I., Lehmann, H.-R., Johanning, D., Seifert, W., and Wagner, C.-U. (1984) Results of the Langmuir probe experiment on board Intercosmos-18. *Proc. Conference on Achievements of the IMS*, Graz, Austria (June 1984). ESA report SP-217, p. 349.

Collis, P. N. and Häggström, I. (1988) Plasma convection and auroral precipitation processes associated with the main ionospheric trough at high latitudes. *J. Atmos. Terr. Phys.* **50**, 389.

Halcrow, B. W. and Nisbet, J. S. (1977) A model of F2 peak electron densities in the main trough region of the ionosphere. *Radio Sci.* **12**, 825.

Hargreaves, J. K. and Burns., C. J. (1996) Electron content measurement in the auroral zone using GPS: observations of the main trough and a survey of the degree of irregularity in summer. *J. Atmos. Terr. Phys.* **58**, 1449.

Jones, D. G., Walker, I. K., and Kersley, L. (1997) Structure of the poleward wall of the trough and the inclination of the geomagnetic field above the EISCAT radar. *Ann. Geophysicae* **15**, 740.

Kavanagh, L. D., Freeman, L. W., and Chen, A. J. (1968) Plasma flow in the magnetosphere. *J. Geophys. Res.* **73**, 5511.

Kohnlein, W., and Raitt, W. J. (1977) Position of the mid-latitude trough in the topside ionosphere as deduced from ESRO 4 observations. *Planet. Space Sci.* **25**, 600.

Liszka, L. (1967) The high-latitude trough in ionospheric electron content. *J. Atmos. Terr. Phys.* **29**, 1243.

Mallis, M. and Essex, E. A. (1993) Diurnal and seasonal variability of the southern-hemisphere main ionospheric trough from differential-phase measurements. *J. Atmos. Terr. Phys.* **55**, 1021.

Moffett, R. J. and Quegan, S. (1983) The mid-latitude trough in the electron concentration of the ionospheric F-layer: a review of observations and modelling. *J. Atmos. Terr. Phys.* **45**, 315.

Muldrew, D. B. (1965) F-layer ionization troughs deduced from Alouette data. *J. Geophys. Res.* **70**, 2635.

Pike, C. P., Whalen, J. A., and Buchau, J. (1977) A 12-hour case study of auroral phenomena in the midnight sector: F layer and 6300 Å measurements. *J. Geophys. Res.* **82**, 3547.

Rodger, A. S., Brace, L. H., Hoegy, W. R., and Winningham. J. D. (1986) The poleward edge of the mid-latitude trough – its formation, orientation and dynamics. *J. Atmos. Terr. Phys.* **48**, 715.

Rodger, A. S., Moffett, R. J., and Quegan, S. (1992) The role of ion drift in the formation of ionisation troughs in the mid- and high-latitude ionosphere – a review. *J. Atmos. Terr. Phys.* **54**, 1.

Rycroft, M. J. and Burnell, S. J. (1970) Statistical analysis of movements of the ionospheric trough and the plasmapause. *J. Geophys. Res*. **75**, 5600.

Spiro, R. W. (1978) A study of plasma flow in the mid-latitude ionization trough. Ph.D. thesis, University of Texas at Dallas, Richardson, Texas.

Thomas, J. O., Rycroft, M. J., Colin, L., and Chan, K. L. (1966) The topside ionosphere. 2. Experimental results from the Alouette 1 satellite. In *Electron Density Profiles in Ionosphere and Exosphere*, p. 322. Amsterdam, North-Holland.

5.5 Troughs and holes at high latitude

Brinton, H. C., Grebowsky, J. M., and Brace, L. H. (1978) The high-latitude winter F region at 300 km: thermal plasma observations from AE-C. *J. Geophys. Res.* **83**, 4767.

Rodger, A. S., Moffett, R. J., and Quegan, S. (1992) The role of ion drift in the formation of ionisation troughs in the mid- and high-latitude ionosphere – a review. *J. Atmos. Terr. Phys.* **54**, 1.